RUSSIAN CHEMICAL REVIEWS
Uspekhi Khimii

March 1978

Translated from *Uspekhi Khimii*, 47, 385-427 (1978)

U.D.C. 537.226.536.421.1

The Formation of High-temperature Materials by Direct High-frequency Fusion in a Cold Container

V.I.Aleksandrov, V.V.Osikov, A.M.Prokhorov, and V.M.Tatarintsev

A new technology of the formation of high-temperature non-metallic crystals, glasses, and fused ceramic materials is described. It is based on the method of direct induction fusion in a cold container. An account is given of the physical foundations of the technology and the technological apparatus is described. The possibilities and advantages of the new technology in the synthesis of pure high-temperature compounds in melts, in the growing of single crystals of oxide compounds, and in the preparation of high-temperature glasses and polycrystalline fused ceramics are demonstrated. The properties of the new materials are described. The bibliography includes 83 references.

CONTENTS

I.	Introduction	213
II.	The technique of direct high-frequency fusion in a cold container. Physical principles, apparatus, and elements of the technology	215
III.	The cold container—an effective chemical reactor	220
IV.	The formation of single crystals. The growing of leucosapphire and ruby crystals	221
V.	The preparation and properties of crystals of stabilised cubic zirconium and hafnium dioxides (fianits)	224
VI.	Preparation of high-temperature glasses	230
VII.	The preparation and properties of fused polycrystalline ceramic materials	232

I. INTRODUCTION

Single crystals, glasses, and fused ceramic materials based on non-metallic high-temperature compounds are widely used in modern engineering and industry. The components of optical apparatus, the working elements of lasers and masers, the refractory components of metallurgical apparatus and glass furnaces, the elements of electrothermal devices, electrodes, and insulating elements of magnetohydrodynamic current generators represent a by no means complete list of the applications of high-temperature non-metallic materials. In this review the term "high-temperature materials" is understood to include not only materials capable of operating at high temperatures (1500° C and above) but also materials obtained at a high temperature regardless of the temperature at which they are subsequently employed. Materials of this type include single crystals, glasses, and polycrystalline ceramics based on oxides, fluorides, nitrides, borides, and certain other compounds.

The technology of high-temperature materials is an independent branch of engineering with its own methods, apparatus, and unsolved problems. The latter include (1 the formation of new single crystals, glasses, and fused

ceramics requiring for this purpose temperatures in excess of 2000° C, necessitating the development of fundamentally new technological processes; (2) the formation of single crystals with an ideally homogeneous crystal structure; this condition requires that the technological processes be performed with parameters effectively stabilised over a long period; (3) the formation of single crystals, glasses, and fused ceramics with high chemical purity; thus the majority of laser crystals and glasses must not contain admixtures of iron, copper, certain lanthanides, and certain other impurities in amounts exceeding 10^{-4}%, while glasses for optical fibre connectors must not contain certain optically active impurities in amounts greater than 10^{-6}%; this condition necessitates the development of special "pure" technological processes in which the initial specially pure reagents are not contaminated; (4) the formation of materials under specific oxidation-reduction condition; (5) the formation of such materials in large amounts with the minimum expenditure of natural resources—energy, water, etc., and also with the minimum amount of waste.

A particular difficulty faced by technologists does not arise from each of the individual problems described but from their combination. For example, a high temperature can be readily achieved in industrial arc fusion processes, but in this method of fusion it is difficult to maintain the chemical purity of the material, to establish the necessary oxidation-reduction conditions, and to ensure the stability of the crystallisation process. On the other hand, fusion with the aid of radiation beams fully ensures a high purity of the material and the required oxidation-reduction conditions, but it is impossible to obtain large amounts of the material. Other existing technological processes which serve as the basis of the synthesis of high-temperature materials can also be shown to have weak features. We shall examine, for example, the existing process for the growing of high-temperature single crystals. Single crystals are most frequently grown from the melt by the Czochralski method[1] involving drawing on a seed. An amount of the crystallisable substance is placed in a metallic crucible heated in a resistance furnace or by high-frequency currents. The crucible plays the role not only of the container but also of a heating body from which heat is transferred to the melt. This method yields many crystals used in modern engineering—the yttrium–aluminium garnet, ruby, leucosapphire, lithium niobate and tantalate, the gadolinium–gallium garnet, lanthanum fluoride, and many others. A weak feature of this technology is the crucible, the choice of materials for the manufacture of which is very limited. These are platinum-group metals: platinum (m.p.1769° C), iridium (m.p.2450° C), and platinum–rhodium alloys (m.p. 1769–1950° C). In a few instances it is possible to employ molybdenum (m.p.2700° C), tungsten (m.p.3400° C), or graphite. The material of the crucible must be more refractory than the material contained in it and it must not interact chemically with the melt and the atmosphere surrounding it. Unfortunately, none of the materials enumerated above possesses the entire set of the necessary properties and this creates serious obstacles to the development of the technology of high-temperature crystals. An analogous problem arises also in the technology of glasses and fused ceramic materials.

We believe that the technology discussed in this review may claim to provide a general solution to the problem of the formation of high-temperature materials from the melt. It is based on the method of direct high-frequency fusion in a cold container. The process includes three principal elements: (1) induction fusion of the substance by high-frequency currents; (2) the retention of the melt in a cold shell having the same composition as the melt; (3) initiation of the process by a special procedure—start fusion.

These elements have been proposed independently at different times by different investigators. Thus it was suggested in 1905 that metals be fused in a solid shell of the same metal[2]. The idea proved so fruitful that it initiated the wide-scale incorporation of garnissage fusion in pyrometallurgy. An electric arc, an electron beam, or a plasma flame were suggested as the energy sources for the fusion of the metal[3]. Induction fusion of the metal in a cold container was proposed later[4,5], but, for reasons which will be described below, this procedure was not introduced on a large scale. Attempts were also made to employ high-frequency fusion in a garnissage in order to obtain semiconductors[6,7]. The idea of employing induction heating in a shell of the solid phase also for high-temperature electrically non-conducting or weakly conducting (in the solid state) materials arose a comparatively long time ago. In 1961 Monforte[8] achieved the fusion of ferrites: Clark and Chapman[9] described the preparation of crystalline uranium dioxide blocks; the relevant patents have been published[10,11]. In the USSR an attempt of this kind was made[12] to obtain crystals of iron-containing garnets.

In the middle 1960's studies designed to create the technology of high-temperature materials based on direct high-frequency fusion, the development of the necessary apparatus, and the synthesis of individual materials were begun at the Lebedev Physical Institute of the USSR Academy of Sciences[13–15]. The first apparatus for the fusion of high-temperature non-conducting (in the solid state) substances become available at the Physical Institute at that time and the fundamental characteristics of the process were understood. At the same time the search was begun for conditions corresponding to the fusion and crystallisation of compounds of different classes fluorides, halides, oxides, and complex oxide compounds. The conditions for the preparation of single crystals, glasses, fused ceramic materials, including multiphase compositions, were investigated. Ruby and leucosapphire single crystals, grown by drawing on a seed became available; single crystals of stabilised cubic zirconium and hafnium dioxides (fianits) were obtained for the first time as well as small single crystals of scandium, yttrium, gadolinium, and erbium oxides. Many fused high-temperature compounds were obtained and their properties proved to be more effective than those of the analogous materials prepared previously by solid-phase synthesis. Among these mention must be made of compounds such as mullite, β-sodium-alumina, yttrium, lanthanum, and other lanthanide chromites, the titanates, zirconates, and hafnates of Group II and III elements, high-temperature glasses, and other materials. The first attempts already showed that the new technology has many advantages.

1. The process temperature has no apparent limitations and may reach 3000° C and above.

2. The absence of contact between the melt and chemically different substances guarantees a high "purity" of the process. The materials obtained have a chemical purity which is at least not inferior to that of the initial components. In many instances the purity actually proves to be higher, because volatile impurities such as the oxides of alkali metals, chlorides, nitrates, sulphates and certain others are burnt off at a high temperature.

3. The processes may be carried out in various gaseous atmospheres: in air, in oxygen, in hydrogen, in neutral gases, and also *in vacuo*, which makes it possible to establish various oxidation-reduction conditions and to carry out oxidative, reductive, or neutral fusion of the materials.

4. The process is very convenient for carrying out chemical reactions in the melt at high temperatures, for example, in the synthesis of complex oxide compounds. Virtually any type of chemical reactions with participation of a melt in both single-phase and heterophase systems can be achieved.

5. The fusion and crystallisation process can be carried out not only periodically but also continuously.

The sum of the above advantages shows that there are good reasons for devising a universal industrial process for the synthesis of high-temperature single crystals, glasses, and fused ceramic materials.

The reports published in recent years have shown that the new technique for the fusion of high-temperature materials is widely used both in the USSR[16] and abroad. For example, it appears that advances have been made in researches of this kind in the USA, where the fusion and crystallisation of zirconium dioxide[17] and certain other high-temperature materials have been achieved at the CERES Company under Wenckus' supervision and at the Bell Laboratories.

II. THE TECHNIQUE OF DIRECT HIGH-FREQUENCY FUSION IN A COLD CONTAINER. PHYSICAL PRINCIPLES, APPARATUS, AND ELEMENTS OF THE TECHNOLOGY

The theory of the heating of materials in an alternating electromagnetic field has been developed in detail[18-20]. Here we shall merely quote the conclusions of the theory, which will assist us in subsequent understanding of the characteristic features of the high-frequency heating of non-metallic high-temperature materials.

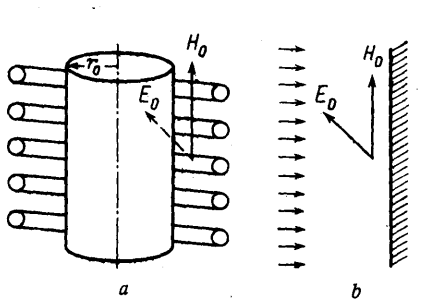


Figure 1. Schematic explanation of the heating of electrically conducting materials by high-frequency currents: *a*) semi-infinite cylinder in a cylindrical electromagnetic field; *b*) interaction of planar electromagnetic waves with a planar semi-infinite object.

Fig. 1 presents a typical scheme which explains the heating of electrically conducting bodies by a high-frequency current. A cylindrical body of the conducting material is in an alternating electromagnetic field with a cylindrical configuration established by a multiturn inductor. The efficiency of the heating of the cylinder depends on the nature of the energy of the high-frequency field absorbed and is determined both by the electrical and magnetic properties of the material, on the one hand, and the frequency of the alternating electromagnetic field, on the other.

In order to derive formulae relating the electric and magnetic field strengths in the material and the energy flux, on the one hand, to the electrical conductivity and the magnetic permeability of the substance, on the other, use is made of Maxwell's equations. The displacement current is neglected assuming that it is small compared with the conduction current. This approximation is undoubtedly valid for metals and is not unduly rough for the class of materials considered here. If the simpler case of the interaction of a planar electromagnetic wave with a planar half-bounded body (Fig. 1*b*) is considered, then, after transformation of Maxwell's equations and the conversion of the vector form into the coordinate form, it is possible to obtain the law governing the decrease of the amplitudes of the magnetic and electromagnetic field strengths:

$$H_{\text{ampl}} = H_0 e^{-\frac{z}{\Delta}} \text{ and } E_{\text{ampl}} = H_0 \frac{\sqrt{2}\, e^{-\frac{z}{\Delta}}}{\gamma\Delta},$$

where H_0 is the amplitude of the magnetic field strength on the surface of the body, z the distance from the surface (depth), γ the specific conductance of the body, and Δ a quantity characterising the attenuation of the amplitudes of E and H; the last quantity is equal to the thickness of the layer in which H_{ampl} and E_{ampl} diminish by the factor e and is called the depth of penetration. It has been shown that

$$\Delta = 5{,}03 \cdot 10^3 \sqrt{\frac{\rho}{\mu_r f}} \text{ (cm)}, \qquad (1)$$

where ρ is the resistivity of the material, μ_r its magnetic permeability, and f the frequency of the electromagnetic field. The flux of the active energy in the body at a depth z also depends on Δ:

$$S_a = H_0^2 \frac{e^{-\frac{z}{\Delta}}}{2\gamma\Delta}. \qquad (2)$$

After substituting $z = 0$ and $z = \Delta$ in this formula, we find that the energy $S_{0a} - S_{\Delta a} = 0.864\, H_0^2/2\gamma\Delta = 0.864\, S_{0a}$ is evolved in a layer of material with a thickness Δ. This justifies the assumption in technical calculations that virtually the entire energy of the high-frequency field is absorbed in a surface layer with a thickness Δ.

We now return to the scheme in Fig. 1*a*. The law governing the attenuation of H, E, and S with increasing depth is derived in the same way as for the planar case (Fig. 1*b*) with the sole difference that the vector form of the equations is transformed into the coordinate form using a cylindrical coordinate system. In the "cylindrical" case the distribution of H, E, and S with respect to the radius of the cylinder at a specified field frequency f is no longer determined by the quantity Δ but by the ratio $r_0\sqrt{2}/\Delta$, where r_0 is the radius of the cylinder and Δ has the same significance as for the planar case. This makes it possible to tabulate data for the depth of penetration of fields into different materials. One should note that the depth of penetration of the electromagnetic wave into the cylinder is determined by the radius of the latter, apart

from the properties of the material and the field frequency. One must therefore recall that Δ for a cylinder is not the true depth of penetration. It has been shown that, for $r_0\sqrt{2}/\Delta > 10$, the functions $H(r)$, $E(r)$, and $S(r)$ are of the same type as for the planar case. When $r_0\sqrt{2}/\Delta < 10$, special methods, which have been described in detail[18], must be used to derive the laws governing the distribution of H, E, and S in the cylinder. We shall not examine specific instances of the interaction of the high-frequency field with bodies having different configurations, since we should then inevitably enter the field of technical calculations, which is of only specialised interest (particularly since gross assumptions are made in these calculations, the main one being failure to take into account the finite length of the cylindrical body, i.e. failure to take into account end effects).

Table 1. Specific conductances of certain solid and fused non-metallic materials.

Compound	State	Temp., °C	Specific conductance, Ω cm	Ingot
LiF	melt	900	$1.2\cdot10^{-1}$	21
NaF	melt	1020	$1.9\cdot10^{-1}$	21
KF	melt	900	$2.6\cdot10^{-1}$	21
NaCl	melt	800	$3.3\cdot10^{-1}$	21
MgO	solid	2000	$5\cdot10^{3}$	22
SiO_2	solid	1700	$9\cdot10^{3}$	22
ZrO_2	solid	2000	1	22
Y_2O_3	melt	2430	$5\cdot10^{-2}$	23
Y_2O_3	solid	1500	$3\cdot10^{1}$	79
Al_2O_3	solid	1875	$2.2\cdot10^{4}$	22
Al_2O_3	melt	2200	$1\cdot10^{-1}$	24

In order to assess the possibility of the high-frequency fusion of non-metallic high-temperature materials (oxides, fluorides, halides, etc.), it is necessary to know the electrical properties of these materials in the solid state and in the melt. Since the vast majority of materials of this kind are non-magnetic, $\mu_r = 1$. Unfortunately the available literature data are extremely scanty. Table 1 presents the electrical conductivities of certain solids and fused non-metallic materials[21-24]. Evidently materials of the type in which we are interested have resistivities in the range 0.01–100 Ω cm at temperatures close to the melting point; on fusion, the conductivities of the materials increase, the increase being pronounced in many instances. It is also seen that at low temperatures their resistivities are 10^4–10^{14} Ω cm, i.e. they are effective dielectrics. Fig. 2*a* illustrates the temperature variation of the resistivity of alumina in the solid (corundum) and fused states, obtained in air[24]. Evidently the resistivity decreased on fusion by more than two orders of magnitude and amounted to 0.1 Ω cm in the melt. Fig. 3 presents a family of $\Delta = (\rho)$ curves for various electromagnetic field frequencies, calculated by Eqn. (1). Using Fig. 3, it is possible to determine the frequencies required to heat the chosen material. For example, a high-frequency generator with a frequency ranging from 500 kHz to 10 MHz should be used for an alumina melt; the depth of penetration then has reasonable values in the range 2.2–0.5 cm. Fig. 3 leads to the conclusion that the range of substances which can be fused by the induction method is restricted to those with resistivities in the melt of approximately 10 Ω cm. Otherwise the required frequencies are outside technically reasonable limits.

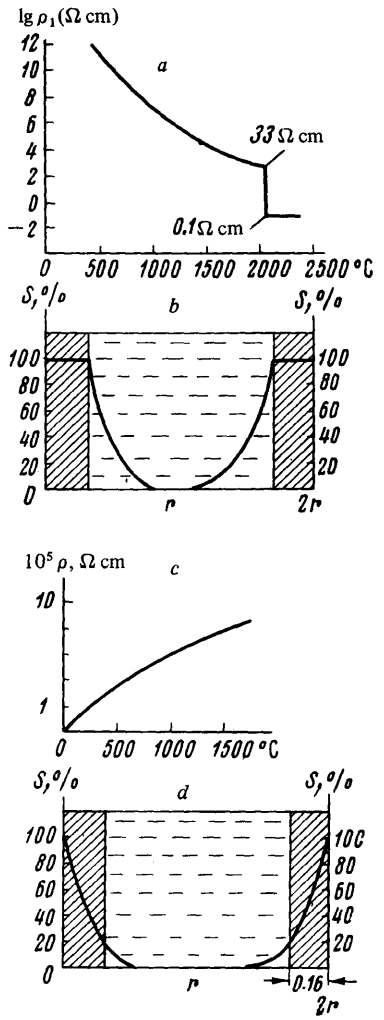


Figure 2. Temperature variation of the resistivity (ρ) and radial distribution of the energy of the high-frequency field (S) absorbed by a two-layer cylinder consisting of solid (outer shaded layer) and liquid (inner region) phases having identical chemical compositions: *a*) alumina; *b*) steel; *c*) Al_2O_3 cylinder, electromagnetic field frequency 5 MHz; *d*) steel cylinder, electromagnetic field frequency 2500 Hz.

The above discussion shows that (1) the melts of the majority of non-metallic high-temperature compounds can be effectively heated by high-frequency currents with the aid of accessible technical means; (2) the heating of these substances from room temperature to the melting point directly by the high-frequency field cannot be achieved.

We shall now consider certain characteristics of the direct high-frequency heating of non-metallic materials in a cold container which follow from the electrical properties of materials of this type. Fig. 2 compares typical tem-

perature variations of the resistivities of a non-metallic material which is a dielectric in the solid state (Fig. 2*a*) and of a metal (Fig. 2*b*). The fundamental difference between these two types of materials is clear from the figures: in the first case the resistivity of the melt is lower by several orders of magnitude than that of the solid phase, while in the second case the resistivity of the melt is higher than that of the solid metal. Figs. 2*c* and 2*d* illustrate schematically for the two instances the nature of the absorption of the energy of the high-frequency field by a double-layer cylinder, the outer shell of which consists of the solid phase and the inner part is occupied by a melt having the same composition as the shell. This model reflects exactly the situation in which we are interested. Since the resistivity of the solid shell is lower than that of the melt in the case of the metal, it follows that, in conformity with Eqns. (1) and (2), it absorbs the major part of the energy of the high frequency field and shields the melt (Fig. 2*d*). The situation is different for a material with a "descending" temperature variation of the resistivity. Here the solid phase is in essence "transparent" to the electromagnetic field and does not prevent its penetration into the melt, while it is not itself heated by the field (Fig. 2*c*). Thus direct induction heating in a cold container is, as it were, specially designed for materials with a descending electrical resistivity–temperature curve and is relatively unsuitable for metals. In direct high-frequency fusion the metal melts in its entirety and a solid shell between the melt and the cold container does not remain, which naturally deprives this technique of its attractive feature—chemical purity; high-frequency fusion of non-metallic materials is free from this disadvantage. The "favourable" distribution of the power generated always leaves, between the melt heated to a high temperature and the cooled container, a layer of the solid phase unheated by the field where the entire temperature difference is "quenched". As will be shown below, this finding makes direct high-frequency fusion of non-metallic materials in a cold container energetically convenient.

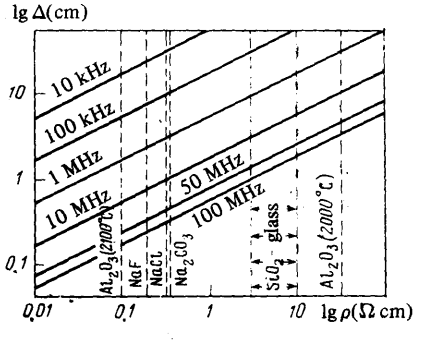


Figure 3. Family of $\Delta = \varphi(\rho)$ curves for various frequencies of the electromagnetic field.

Thus the high-frequency fusion of refractory dielectrics can be divided into two components: the heating of the material from room temperature to the melting point (which cannot be achieved directly by the induction method) and the maintenance of the substance in a fused state by supplying the energy of the high-frequency field. We shall examine the first component, the so called start fusion process (Fig. 4*a*). In the first place we shall determine the amount of the initial solid material which must be fused to enable the resulting melt to be heated by the field and grow in volume. A condition for its "viability" is the inequality

$$V \cdot P > K (T_m - T_0) \pi D^2, \qquad (3)$$

where V is the volume of the starting melt, P the power absorbed by unit volume of the melt, K the coefficient of heat transfer from the melt to the heat exchanger (the cooling water), T_m the temperature of the melt, T_0 the temperature of the heat exchanger, and D the drop diameter. The heat of the phase transition is excluded from consideration, because the fusion process can be carried out in principle as slowly as desired. For a drop diameter D much smaller than the internal diameter of the container, the assumption that the specific absorbed power P remains constant is not unduly approximate. We obtain from formula (3) the expression

$$D > \frac{6K}{P}(T_m - T_0). \qquad (4)$$

The above inequality shows that, for the specified electromagnetic field strength and electrical conductivity of the melt (they determine the value of P), the critical dimension of the drop of the melt depends mainly on the thermally insulating properties of the solid phase. Thus, having satisfied condition (4), we obtain a "viable" drop of the melt, which absorbs the energy of the high-frequency field and increases in size as a result of the fusion of the surrounding solid phase.

In order to answer the question whether the fusion process proceeds until the complete fusion of the entire solid phase or ceases at some stage, we shall examine the condition for phase equilibrium, i.e. for the spatial stability of the interface between the melt and the solid phase (Fig. 4*b*). Phase equilibrium implies that the temperature at any point on the interface is equal to the melting point (T_{fu}) and does not vary with time. The amount of heat given up by the melt to the solid wall (on the assumption of complete mixing of the melt) is $Q_1 = \alpha_1(T_m - T_b)F\tau$, where α_1 is the heat transfer coefficient, T_b the temperature at the boundary between the solid and liquid phases, F the heat transfer surface area, and τ the time. The amount of heat transferred through the layer of the solid phase with a thickness σ_S and a thermal conductivity λ to the heat exchanger is $Q_2 = (\lambda/\sigma_S)(T_b - T_0)F\tau$. In the steady state $T_b = T_m$ and $Q_1 = Q_2$. We then obtain $\alpha(T_m - T_{fu})(\lambda/\sigma)(T_m - T_0)$ or

$$\frac{\lambda}{\sigma_s \alpha} = \frac{T_m - T_{fu}}{T_{fu} - T_0}, \qquad (5)$$

where $T_m - T_{fu} = \Delta T$—a quantity characterising the superheating of the melt. When $\Delta T \to 0$, we have $\sigma_S \to \infty$, which implies that the melt must be superheated in order to maintain the phase equilibrium. We shall assume that λ, α, and T_0 are independent of σ_S, whereupon

$$\sigma_s \Delta T = \text{const}. \qquad (6)$$

It is seen from Eqns. (5) and (6) that the system responds by a decrease or increase of the thickness of the layer of solid phase to an increase or decrease of T_m. On the other hand, the complete fusion of the solid phase

requires infinite superheating. Furthermore, any processes in the solid shell leading to a change in its thermal conductivity (for example sintering) disturb the phase equilibrium and require a change either in the temperature of the melt or in the thickness of the solid layer. The state of phase equilibrium is also influenced by the nature of the mixing of the melt, which determines the coefficient of heat transfer. The requirement for superheating, which determines the very existence of the melt in the scheme under consideration, constitutes a marked difference between the cold container and the heated crucibles usually employed: in the latter case the temperature of the melt may be made as close as desired to that of the melting point and in certain cases the melt is actually supercooled. The inevitable superheating of the melt in the cold container has certain important consequences in its crystallisation, particularly in the growing of single crystals (see below).

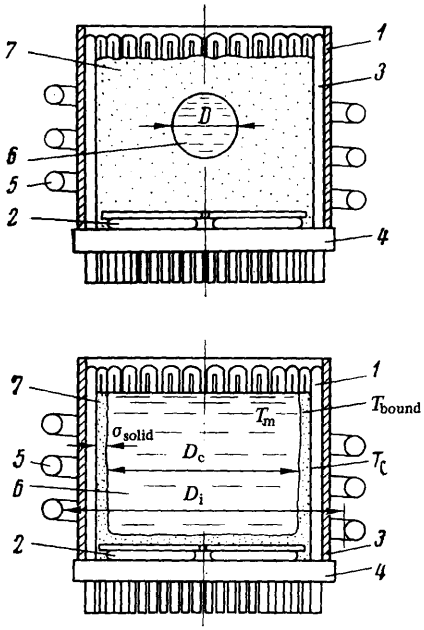


Figure 4. Schematic illustration of fusion (*a*) and of the state of equilibrium in the melt–solid system (*b*) in a cold container: 1) tubular water-cooled element; 2) water-cooled bottom; 3) insulating quartz cylinder; 4) retaining ring made of an insulating material; 5) inductor of the high-frequency generator; 6) melt; 7) charge.

We shall discuss further yet another important characteristic of the cold container–solid shell–melt system. We shall examine how the system responds to a decrease in the power ΔP absorbed by the melt (caused, for example, by the uncontrolled decrease of the power of the high-frequency generator). The decrease of the power immediately causes a decrease of T_m, which disturbs the phase equilibrium: the thickness of the solid shell begins to increase—the ratio of the diameter of the charge (D_c) to that of the inductor (D_i) diminishes. Under these conditions, either (1) a new state of equilibrium is established with a larger value of σ_S or (2) uncontrolled complete setting of the melt takes place. The point is that, with increase of σ_S, there is a simultaneous diminution of the diameter of the region of the melt which constitutes the charge in the inductor of the high-frequency generator; the coupling with the inductor diminishes at the same time. On the other hand, with increase of the thickness of the solid shell, the thermal insulation also increases and the heat flux from the melt in the cold container diminishes. The laws governing the decrease of the power absorbed by the melt and of the heat losses under these conditions are different. Figs. 5*a* and 5*b* represent schematically two possible versions of the response of the system to the decrease of the power of the generator. The result is to a large extent determined by the thermal conductivity of the solid phase: the higher the thermal conductivity the less stable the system. The occurrence of the spatial instability of the phase boundary during high frequency fusion of high-temperature non-metallic materials is a new factor which specialists working in the field of the high-frequency heating of metals did not encounter. This effect has a major influence on the apparatus and technological conditions in the fusion and crystallisation of specific high-temperature materials.

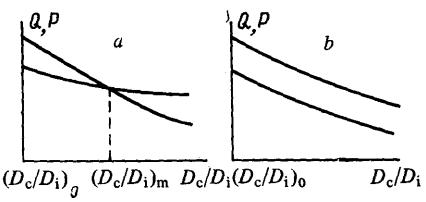


Figure 5. Response of the melt–solid phase system in a cold container to the decrease of the power of the generator: *a*) stable system; *b*) unstable system (D_m = melt diameter; D_i = inductor diameter).

Several types of apparatus have been developed at the Lebedev Physical Institute of the USSR Academy of Sciences for the direct high-frequency fusion and crystallisation of non-metallic high-temperature materials[13–15]. Each type of apparatus consists of a high-frequency generator with an oscillatory power ranging from 10 to 80 kW and a frequency from 1 to 13 MHz, a working chamber with water-cooled walls, a container, and a system for the stabilisation of the power of the generator and of the flow of cooling water. The high-frequency generator can be used in conjunction with both single-circuit and two-circuit schemes. Its characteristic feature is that it must be capable of stable operation at the maximum potential under the conditions of sharp changes in the charge: virtually in the range from its complete absence (at the start fusion stage) to the maximum charge. The working chamber serves to establish the required atmosphere (inert gas, reducing, or oxidising atmosphere). In order to maintain a constant average temperature of the melt and the phase equilibrium in the melt–solid shell system, devices stabilising the anodic potential (or the heater of the generator electronic valve) and the stream of cooling water are used.

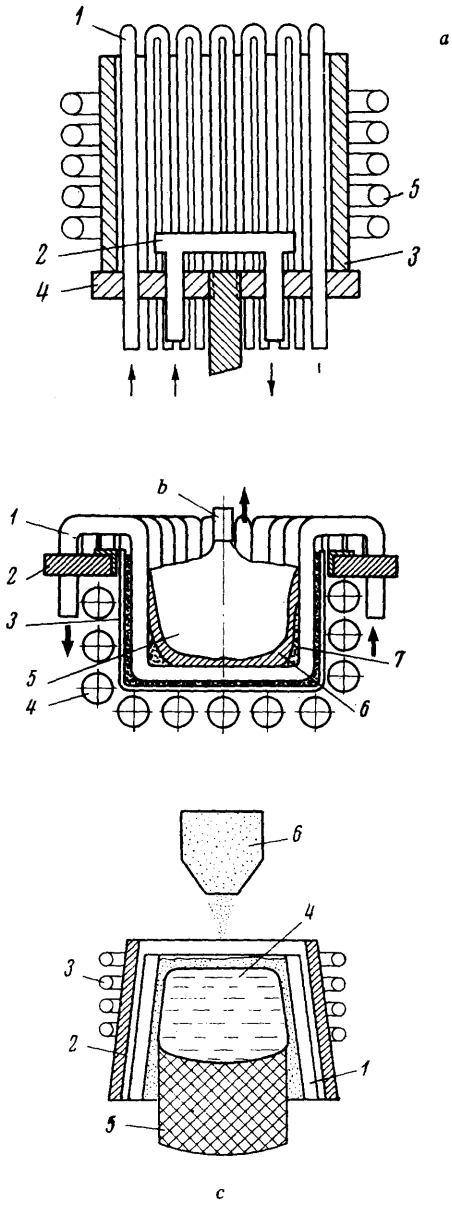


Figure 6. Design of cold containers: *a*) multielement cold container for the periodic fusion and crystallisation of refractory non-metallic materials [1) tubular water-cooled element; 2) water-cooled bottom; 3) insulating quartz cylinder; 4) insulating Micalex ring; 5) inductor of high-frequency generator]; *b*) multielement cold container for the periodic fusion and crystallisation of refractory non-metallic materials with a thermal conductivity in the solid state exceeding 6 W m^{-1} K^{-1} [1) tubular water-cooled element; 2) insulating Micalex insulating ring; 3) insulating quartz beaker; 4) inductor of high-frequency generator; 5) melt; 6) layer of crystallised melt; 7) charge; 8) growing crystal]; *c*) multielement cold container for the continuous fusion and crystallisation of refractory non-metallic materials [1) double-walled water-cooled conical container; 2) insulating quartz shield; 3) inductor of high-frequency generator; 4) melt; 5) block of crystallised material; 6) hopper with charge].

The design of the cooled container must meet a number of special requirements. In the first place, since the energy source is outside the container, the latter must be "transparent" to the energy.

Table 2. Compounds fused in a cold container.

Compound	M.p., °C	Compound	M.p., °C	Compound	M.p., °C
LiF	842	La_2O_3	2230	Lu_2O_3	2470
NaF	995	CeO_2	—	TiO_2	1855
CaF_2	1403	Pr_6O_{11}	2040	ZrO_2	2690
NaCl	800	Nd_2O_3	2315	HfO_2	2790
KCl	770	Sm_2O_3	2320	V_2O_5	670
MgO	2880	Gd_2O_3	2395	Nb_2O_5	1510
CaO	2585	Tb_4O_7	2330	Ta_2O_5	1877
SrO	2430	Dy_2O_3	2485	Bi_2O_3	817
BaO	1923	Ho_2O_3	2395	Cr_2O_3	2300
$Al_2O_3^*$	2046	$Er_2O_3^*$	2400	MnO_x	1700
$Sc_2O_3^*$	2405	Tm_2O_3	2390	Na_2CO_3	851
$Y_2O_3^*$	2410	Yb_2O_3	2420		

*Single crystals were obtained.

Table 3.

Compound	M.p., °C	Temp. of synthesis, °C
$Na_2O \cdot 11Al_2O_3$	1923	1970
$MgO + Al_2O_3 \rightarrow MgAl_2O_4$	2130	2300
$CaO + Al_2O_3 \rightarrow CaAl_2O_4$	1600	2300
$BaO + Al_2O_3 \rightarrow BaAl_2O_4$	2000	2300
$3Y_2O_3 + 5Al_2O_3 \rightarrow 2Y_3Al_5O_{12}^*$	1930	2100
$La_2O_3 + Al_2O_3 \rightarrow 2LaAlO_3$	2100	2300
$3Al_2O_3 + 2SiO_2 \rightarrow 3Al_2O_3 \cdot 2SiO_2$	1910	2100
$2Al_2O_3 + SiO_2 \rightarrow 2Al_2O_3 \cdot SiO_2$	1850	2100
$SrO + TiO_2 \rightarrow SrTiO_3$	2038	2200
$R_2O_3 + 2TiO_2 \rightarrow R_2Ti_2O_7^*$ (R = Sc, Y, La, Nd, Sm, Eu, Gd, Dy, Ho, Er, Tm, Yb)	—	2000—2300
$CaO + ZrO_2 \rightarrow CaZrO_3$	2345	2600
$Sc_2O_3 + 2ZrO_2 \rightarrow Sc_2Zr_2O_7^*$	2700	2900
$SrO + ZrO_2 \rightarrow SrZrO_3$	2470	2600
$La_2O_3 + 2ZrO_2 \rightarrow La_2Zr_2O_7$	—	2400
$SrO + HfO_2 \rightarrow SrHfO_3$	—	3000
$Y_2O_3 + Cr_2O_3 \rightarrow 2YCrO_3^{**}$	2290	2500
$MgO + Cr_2O_3 \rightarrow MgCr_2O_4$	2150	2300
$CaO + HfO_2 \rightarrow CaHfO_3$	2700	2900
$La_2O_3 + Cr_2O_3 \rightarrow 2LaCrO_3^{**}$	2430	2600
$CaO + MoO_3 \rightarrow CaMoO_4$	1449	1700
$SrO + MoO_3 \rightarrow SrMoO_4$	1468	1800
$CaO + WO_3 \rightarrow CaWO_4$	1580	1800
$SrO + WO_3 \rightarrow SrWO_4$	1566	1800
ZrO_2 + (8-50 mole%) MgO, CaO, SrO, Sc_2O_3, Y_2O_3, La_2O_3, $TR_2O_3^*$	—	2700—2900
HfO_2 + (8-50 mole%) MgO, CaO, SrO, Sc_2O_3, Y_2O_3, La_2O_3, TR_2O_3	—	2800—3000
$R_2O_3 - Al_2O_3 - SiO_2$ (R = Sc, Y, La, Nd, Sm, Eu, Gd, Tb, Er, Yb)***	—	1800—2400

*Single crystals were obtained.
**With an admixture of 5 wt.% $CaCr_2O_4$.
***Optically transparent glasses.

This means that it must be either made of a dielectric material or, when the container is made of a metal, must have slits which prevent the closure of circuits generating circular currents. Furthermore, the container must be made of a material with a high thermal conductivity and must be vigorously cooled with water (or another heat

exchanger). Several types of containers made of dielectric materials (quartz glass) and various metals (copper, aluminium) were developed at the Physical Institute.

The containers illustrated in Fig. 6 proved to be the most suitable for the fusion and crystallisation of refractory non-metallic materials. One of them (Fig. 6*a*) makes it possible to fuse and crystallise a large number of different materials (Tables 2 and 3). In order to obtain crystals of materials whose thermal conductivity in the solid state is higher than 6 W m^{-1} K^{-1}, it is more useful to use a container of a different type (Fig. 6*b*), which makes it possible to supply energy not only from the lateral surface of the melt but also from below. The container illustrated in Fig. 6*c* is designed for the continuous fusion and crystallisation of materials.

Direct experimental determination of the efficiencies of the above types of apparatus showed that 50–60% of the electrical power supplied to the apparatus is evolved in the container with the melt.

The technological fusion process includes three stages. It begins with the formation of the "seed" melt, which, as stated above, can be achieved only by means of an additional source of heat. The following procedures have been used for this purpose: (1) fusion by supplying radiant energy; (2) fusion with the aid of flames; (3) heating and fusion by means of an electric arc; (4) fusion by introducing into the test substance an extraneous conducting material—the heating body. The most convenient method for the fusion of oxide and certain other types of materials is start fusion based on the use of small amounts (usually several grammes) of a metal whose atoms enter into the composition of the material to be fused: aluminium in the case of alumina, yttrium in the case of yttrium oxide, etc.[14] When the high frequency generator is switched on, the lumps of metal introduced into the charge are heated by the energy of the high frequency field and melt the surrounding charge. As fusion proceeds, the metal is oxidised by atmospheric oxygen and the resulting oxide mixes with the melt without contaminating it. After the critical volume of the starting melt has been exceeded under the influence of the high-frequency field, the entire charge gradually melts with the exception of the layer in contact with the cooled walls of the container. Fresh portions of the charge are added to the melt until the attainment of the required volume. This is the second, transitional stage of the process. As the charge melts, equilibrium is established, which may be maintained indefinitely. This is the third stage of the fusion process. When the high frequency generator is switched off, rapid mass crystallisation or vitrification of the melt takes place and polycrystalline ingots or glasses are obtained. On slow directed crystallisation of the melt by the gradual decrease of the power of the generator or slow lowering of the container with the melt relative to the inductor, it is possible to obtain large single-crystal blocks. Single crystals can also be obtained by drawing on seeds. The crystallisation and glass formation processes will be described in greater detail below in the sections devoted to specific materials.

III. THE COLD CONTAINER—AN EFFECTIVE CHEMICAL REACTOR

The most important element of the technology of high-temperature materials is the chemical synthesis of the compounds, since the majority of the materials are complex compounds: complex oxides, oxygen-containing salt-like substances, complex fluorides, and mixed or simple compounds into which admixtures have been introduced. In order to obtain single crystals, a glass, or a ceramic material, it is necessary to synthesise initially the required compounds from simple starting materials. As a rule, the synthesis is carried out by the method of solid-phase reactions. For this purpose, the starting materials in the form of finely dispersed powders are carefully mixed and then heated at a temperature below the melting point of the reaction product. The temperature is usually 0.5–0.7 of T_{fu}. The mechanism of chemical reactions in the solid phase is complicated[25]. However, regardless of the details, the diffusion of atoms of one of the components (or those of both components) through a layer of the solid reaction products is an inevitable stage. Diffusion coefficients in solids are usually small (10^{-6}–10^{-12} $cm^2 s^{-1}$), so that diffusion is a bottleneck in the solid-phase reaction, restricting its velocity.

Owing to the low rate of solid-phase reactions, the synthesis is long and it is difficult to bring the process to completion, so that the reaction product contains as a rule an admixture of the unreacted components, i.e. it is not homogeneous. In reactions in melts, diffusion is no longer a "bottleneck", because, firstly, its rate in liquids is much higher than in solids and, secondly, liquids can be vigorously stirred either forcibly or by convection, as a result of which the rate of reaction increases still further. Furthermore, liquid reaction products can be subsequently crystallised and their chemical purity and structural perfection can be thereby improved. Despite its obvious advantages, the synthesis of high-temperature compounds in the melt, particularly when compounds with $T_{fu} \simeq 2000^\circ C$ are concerned, is used to a very limited extent. One can mention only a few studies where synthesis in a melt was carried out using a solar furnace[26,27], a rotating plasma furnace[28], or arc furnaces[29].

As already pointed out in the introduction, a cold container in which the melt of the initial substances or reaction products is heated by high-frequency currents can serve as an extremely universal and at the same time "clean" high-temperature chemical reactor. Using this technique, we were able to synthesise many complex oxides. Together with the reaction equations, these compounds are listed in Table 3. Most of the reactions enumerated are coupling reactions and take place in a homogeneous system. However, some of these are of the combined type: together with the interaction of the liquid components, there is a heterogeneous reaction involving the components of the gaseous atmosphere. A relevant example is provided by the solid solution of zirconium and hafnium dioxides which were synthesised[15] and then stabilised by lanthanide or variable-valence transition metal oxides. The rate of the reaction and the form of its products vary as a function of the composition of the gaseous atmosphere. Another example of a combined reaction is the synthesis of solid solutions of yttrium, lanthanum, and other lanthanide chromites with an admixture of magnesium, calcium, strontium, and barium chromites. Depending on the atmosphere, the electrical conductivity of these substances varies sharply.

The study of the kinetics of coupling reactions in melts showed that the chemical interaction of the initial components proceeds at a rate equal to the rate of solution of the particles of the solid components (lumps) in the melt of the reaction products, i.e. actually at the rate of fusion. The rate of fusion in typical instances is 0.1–1.0 kg min^{-1}, depending on the superheating of the melt, its viscosity, and the heat of the phase transition on fusion of the components. Thus the homogeneous chemical equilibrium in the

systems which we investigated is established over a period ranging from several seconds to several minutes. The study of the reaction products by X-ray diffraction, microscope, electron microscope, and spectroscopic methods has invariably shown that, for a strictly stoichiometric composition of the initial mixture of components, the content of the latter in the final product does not exceed 0.01–0.1 vol.%. The kinetic curve for the synthesis in the melt (curve *2*) is compared in Fig. 7 with the corresponding curve for the solid-phase synthesis (curve *1*); the comparison evidently favours the synthesis in the melt.

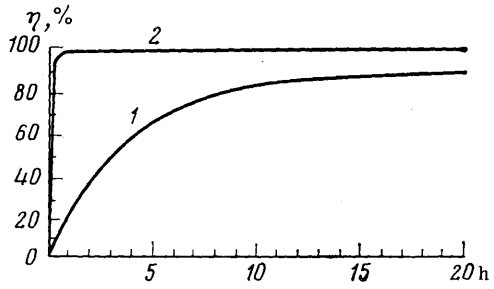


Figure 7. Kinetic curves (yield of reaction product η plotted against time): 1) for reactions in a mixture of three solid phases: $CaCO_3 + Fe_2O_3 \rightarrow CaFe_2O_4$; 2) for the reaction in the melt[25] $CaO + ZrO_2 \rightarrow CaZrO_3$ (the authors' data).

The situation is somewhat more complex in heterophase reactions, where the fused substance reacts with the gaseous atmosphere. Here it is necessary to examine two limiting cases.

(1) The active component of the gaseous atmosphere is insoluble in the melt. In this case the contact surface is restricted to the open surface of the melt. The rate of reaction is limited by the diffusion of gas molecules through the interface and the diffusion of reaction products in the bulk of the melt if the melt is not stirred or if the rate of stirring may be neglected. The viscosity of the melt therefore plays an important role here. The dependence of the rate of equilibration on the viscosity of the melt is clearly revealed when the rates of combustion of the starting metal and the reduction products in melts comprising lanthanum oxide, mullite ($3Al_2O_3.2SiO_2$), and the glass $La_2O_3.Al_2O_3.6SiO_2$ are compared. The viscosity of the melt increases sharply on passing from La_2O_3 to $3Al_2O_3.2SiO_2$ and particularly to a glass. In full conformity with this finding, the rates of combustion of metallic aluminium and the reduction products dispersed in the bulk of the melt are very different. Aluminium is combusted in 5–10 min in the La_2O_3 melt and in 15–20 min in the mullite melt; in a glass melt aluminium is not combusted after 10 h at 2000° C.

(2) The active component of the gaseous atmosphere is soluble in the melt; the rate of the heterophase reaction is then no longer limited by the rate of diffusion of the reaction products. An example of heterophase reactions with vigorous dissolution of the gaseous component is provided by the oxidation of the reduction products and metallic aluminium in Al_2O_3, $YAlO_3$, $Y_3Al_5O_{12}$, $MgAl_2O_4$, and certain other melts. It has been established experimentally that the melts of these substances dissolve large amounts of gaseous oxygen[30]. Thus a melt of alumina in contact with air dissolves more than 40 vol.% of oxygen. In this case the heterophase equilibrium is established after 5 min for a volume of the melt of 0.5 litre. When melts crystallise rapidly, the dissolved oxygen is evolved vigorously, the melt "boils", and the solidified block is threaded by a large number of large pores.

IV. THE FORMATION OF SINGLE CRYSTALS. THE GROWING OF LEUCOSAPPHIRE AND RUBY CRYSTALS

The growing of crystals from a melt in a cold container has many characteristic features compared with the usual method where they are grown in heated crucibles (the Czochralski, Stockbarger, Kiropoulos, or zone crystallisation methods). We shall consider these characteristics in connection with the method of crystallisation of the melt.

The Growing of Crystals by Drawing on a Seed

When crystals are grown by drawing on seeds (in the usual version this involves the Czochralski method) the following conditions must be observed: (1) a strictly defined distribution of temperature in the melt and in the crystallisation front must be established, namely the temperatures in the crystallisation front, i.e. in the middle part of the surface of the melt, must be lower than at any other point in the melt and (2) the temperature in the crystallisation front must be effectively stabilised. Convective streams in the melt play a major role in the distribution of temperature. Figs. 8*a* and 8*b* present photographs of the convection patterns on the surfaces of Al_2O_3 and $3Al_2O_3.2SiO_2$ melts in a cold container. The nature of the pattern depends on the generator frequency, the electrical conductivity of the material, the superheating and viscosity of the melt, and its diameter. The first pattern is typical of the majority of melts which we have investigated. The appearance of an irregular pattern, varying with time, is caused by the bulk-phase nature of the heating owing to the comparatively large depth of penetration by the high frequency field.

The required radial temperature gradient and stabilisation of the convection pattern were achieved by increasing the frequency and the diameter of the melt. Fig. 9 presents a plot of the distribution of temperature on the surface of an Al_2O_3 melt 80 mm in diameter at a field frequency of 5.28 MHz. Evidently in this case the radial temperature gradient satisfies the condition for the growing of crystals by drawing on a seed. However, here too the fluctuations in convective streams over a period of time remain significant. The majority of melts which we obtained had a low viscosity and only some of them, whose compositions incorporated glass-forming components such as SiO_2, were viscous. The absence of a convection pattern on the surface of the $3Al_2O_3.2SiO_2$ melt (Fig. 8*b*) is encountered rarely and is due to the high viscosity of the melt.

The possibility of growing crystals by drawing on a seed depends on the temperature of the melt and the thermal conductivity of the crystal. For normal crystal growth from the melt, it is necessary that the temperature of the latter at the crystallisation front, i.e. under the crystal, should be lower than at other points on the surface of the melt (Fig. 10). This requires that the heat loss from the

surface of the melt under the crystal (Q_1) should exceed the heat loss from the open melt surface (Q_2). At high temperatures Q_2 is determined mainly by the radiation from the surface. Q_1 for "grey" bodies, such as the majority of refractory crystals at a temperature close to the melting point, is determined by the thermal conductivity of the crystal. Normal crystal growth is possible only for $Q_1 > Q_2$; otherwise uncontrolled crystal growth in the tengential direction begins. This effect is encountered in the growing of high-temperature crystals by the Czochralski method. In the case under consideration the situation is aggravated by the fact that, firstly, the melting points of the materials are in many cases 2000° C and above and, secondly, by the fact that, owing to the very essence of the method, superheating of the melt is needed. All these factors lead to considerable radiation losses from the surface of the melt, the attainment of the condition $Q_1 > Q_2$ is hindered, and uncontrolled tangential crystal growth results.

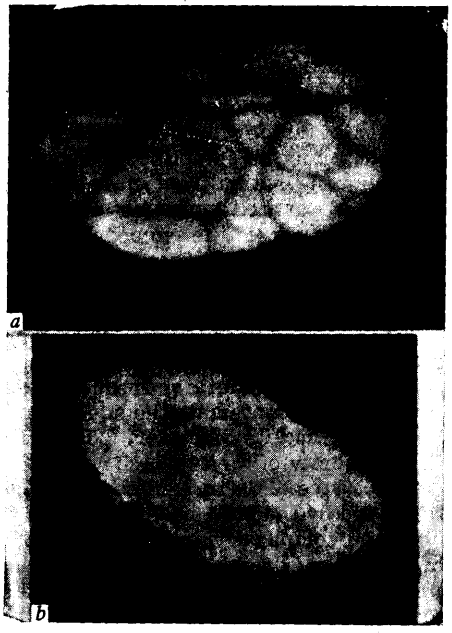


Figure 8. Convection patterns on the surface of the melt: *a*) Al_2O_3; *b*) $3Al_2O_3.2SiO_2$ (mullite).

The Growing of Crystals by Lowering the Crucible

In this case the growing of crystals in a cold container also differs significantly from that in the usual "hot" crucible by the Stockbarger–Bridgman method. The point is that, over the entire interface, the melt is in contact with a polycrystalline phase having the same composition. When the temperature of the melt is reduced, its crystallisation begins immediately at numerous nuclei already present. In this case it is almost impossible to grow a single crystal, since directed crystallisation of a large number of blocks takes place. However, as the growth of crystals proceeds in a large volume of the melt, the number of crystal blocks diminishes owing to selection by virtue of the different rates of growth and, after the complete crystallisation of the melt, the ingot is found to consist of a not unduly large number of single crystals. Thus it is possible to obtain small but quite perfect Sc_2O_3, Y_2O_3, Al_2O_3, and $Y_3Al_5O_{12}$ crystals as well as those of certain other compounds. Best results were achieved when single crystals of stabilised cubic zirconium and hafnium dioxides were grown by this procedure (see below).

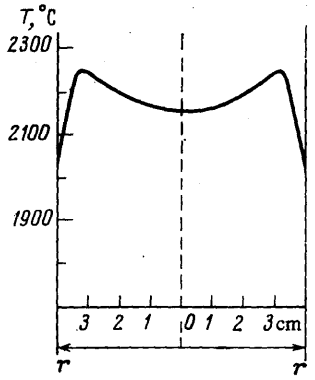


Figure 9. Radial temperature gradient on the surface of an alumina melt.

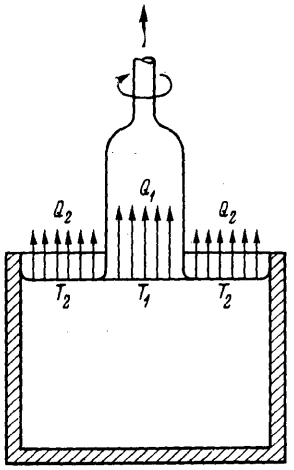


Figure 10. Schematic explanation of the nature of the thermal field in the zone of crystal growth by the Czochralski method.

Growth from Solution in the Melt

When crystals are grown from solutions in melts, the melt is highly superheated in the initial stage. This makes it impossible to employ the cold container technique in its pure form, since the solid shell fuses because of the identity of its composition with that of the melt. The difficulty may be overcome by employing the method used for the first time to grow semiconductor crystals[31], where

the solid shell consists of a cylinder, pressed beforehand, of material having the same composition as the crystallising material (Fig. 11). In this case the saturated and superheated melt is in equilibrium with the solid shell. On the other hand, if the temperature at the solution–solid shell interface is non-uniform at different points, there is a possibility of the transfer of material from hotter to colder regions via the gradual dissolution of the shell and crystallisation of the dissolved material on the nuclei in the colder part of the volume (Fig. 11). Thus crystals may be grown from solutions in melts heated to temperatures much higher than are permitted by the platinum crucibles employed in processes of this kind (~ 1400–1500° C). The chemical corrosiveness of the melt does not play a role in this case. In a broader sense this technique can be used not only for crystallisation but also for the synthesis of substances in heated melts via coupling, substitution, exchange, etc. reactions.

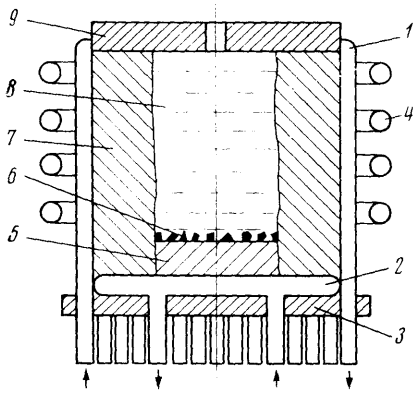


Figure 11. Schematic illustration of crystallisation from solution in a melt in a cold container: 1) tubular water-cooled element; 2) water-cooled bottom; 3) retaining ring of insulating material; 4) inductor of high-frequency generator; 5), 7), and 9) polycrystalline ceramic material having the same composition as the charge; 6) crystals; 8) melt.

On the one hand, the high thermal conductivity of corundum stabilises the crystal growth, ensuring a rapid removal of heat and preventing tangential growth, and, on the other hand, there is rapid removal of heat from the melts through the solid shell to the cold container, which leads (together with the low value of the specific power absorbed by the Al_2O_3 melt) to spatial instability of the interface between melt and the solid shell and to the necessity for high degrees of superheating of the melt. In order to attain prolonged stable growth of sapphire and ruby crystals, we therefore used the containers and inductors illustrated in Fig. 6*b*. This configuration of the container ensures uniform heating of the melts not only from the sides but also from below[14]. Fig. 12 presents a photograph of a growing sapphire crystal. The crystal diameter was regulated by altering the positions of the mobile shields located over the melt. The rate of drawing was 10–30 mm h^{-1} and the rate of rotation varied from 20 to 140 rev min^{-1}. In those cases where the convection pattern fluctuated markedly planetary rotation of the crystals was achieved by means of a special mechanism. During such rotation, the crystal intersects a large number of regions at different temperatures and the temperature of the front is averaged out; optical inhomogeneities associated with the entrainment of oxygen bubbles accordingly disappear. The crystallisation front in such crystals is virtually planar.

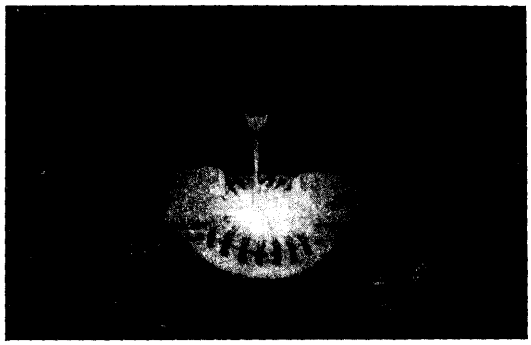


Figure 12. Photograph of a growing sapphire crystal.

The Growing of Sapphire and Ruby Crystals[32–35]

The growing of leucosapphire and ruby crystals in a cold container is to a large degree determined by the following factors: (1) the relatively low electrical conductivity of the Al_2O_3 melt; (2) its low viscosity; (3) the high solubility of gaseous oxygen in the melt; (4) the high thermal conductivity of solid corundum. The first two features lead to the formation of a fluctuating convection pattern generated by the variations in temperature at the crystallisation front. The third feature results in the evolution of oxygen at the boundary with the solid phase during the crystallisation of the oxygen-saturated melt. As a result, under the conditions of small temperature oscillations, small oxygen bubbles are incorporated in the growing crystal and give rise to light scattering regions.

Single crystals of sapphire and ruby with different orientations, up to 160 mm long and up to 35 mm in diameter, were obtained in this way. The crystals have characteristics which follow from the specific features of their preparation. The density of the dislocations in the basal plane was 10^2–10^3 cm^{-2}. A planar crystallisation front leads to a uniform radial distribution of chromium atoms in the ruby crystal. The distribution of chromium along the length of the ruby crystals was inhomogeneous: during the drawing process, the concentration of chromium fell, which is associated with the decomposition of chromium oxide in the melt during its superheating. In order to equalise the concentration of chromium over the length of the crystal, the melt was provided with a programmed "supplementary supply" of powdered chromium oxide from a special bunker was used.

V. THE PREPARATION AND PROPERTIES OF CRYSTALS OF STABILISED CUBIC ZIRCONIUM AND HAFNIUM DIOXIDES (FIANITS)

The monoclinic zirconium and hafnium dioxide crystals, obtained from solutions in the melt, have already been described[36]. The preparation of these crystals by the hydrothermal method is described in another communication[37]. In both cases small crystals several millimetres in size were obtained. The high melting points (Table 2), polymorphic transformations, and the high chemical corrosiveness of the melts precluded the growing of the crystals of these oxides from the melt. We developed a method for obtaining crystals of stabilised cubic zirconium and hafnium dioxides (fianits) from the melt[13,15,38]. The initial components (ZrO_2 and HfO_2) were of "specially pure" grade. The stabilising components were magnesium, calcium, strontium, barium, scandium, yttrium, lanthanum and other lanthanide oxides at concentrations up to 40 mole %.

The charge was placed in a water-cooled copper container (Fig. 6*a*), metallic zirconium, hafnium, or yttrium being used for the start fusion. The crystals were grown at 3000° C by the slow lowering of the container with the melt relative to the inductor. The growth time was 8 h. 1.5–6 kg of single-crystal blocks, up to 8 cm long and with a cross-sectional area up to 10 cm^2, was obtained simultaneously on our apparatus (Fig. 13). The crystals grown in this way were then annealed in vacuum or gas furnaces.

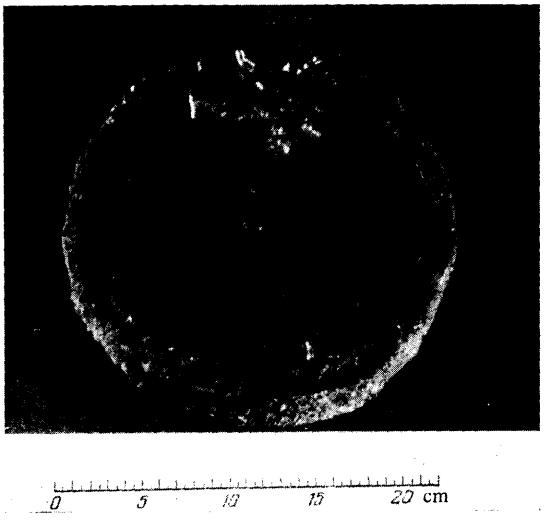


Figure 13. A block of zirconium dioxide crystal.

The Structure of the Crystals

The X-ray diffraction analysis[39] was performed on a DRON-0.5 apparatus using Cu$K\alpha$ radiation. The lattice constant of the crystals of stabilised zirconium dioxide was determined to within 0.001 Å from the (531) peak. The degree of order in the structure was characterised by the ratio of the intensities of the (600) and (200) lines and the normalised widths of the (531) peaks at the level of half their height. According to the results of the X-ray diffraction analysis, the crystals stabilised by X_2O_3 consisted in the main of the stabilised high-temperature crystal form with a cubic lattice of the fluorite structural type. The space group was $^5O_h - Fm3m$. Fig. 14 presents the experimental and calculated lattice constants and the number of vacancies in ZrO_2 as a function of the concentration of the stabilising oxide. The calculation was based on the hypothesis of close-packed spheres of different radii and the following formula was used:

$$d = 2.31\left(R_{Zr} + R_O + \frac{2m\Delta R}{100+m}\right), \qquad (7)$$

where d is the lattice constant, R_{Zr} and R_O are the radii of zirconium and oxygen ions (0.81 and 1.40 A) respectively, m is the concentration of Y_2O_3 (mole %), and ΔR the difference between the radii of yttrium (0.90 Å) and zirconium ions. Eqn. (7) and the plots in Fig. 14 show that the concentration dependence of the lattice constant is not linear. The diffractometer traces for the specimens with 6 mole % Y_2O_3 contain split lines which, together with the deviation of the lattice constant towards higher values, shows that these specimens include both cubic and distorted tetragonal phases. Naturally, under these conditions the Y_2O_3 concentration must be referred solely to the cubic phase, which results in an increase of its lattice constant to 5.136 Å. The content of the tetragonal phase in the specimens can be estimated from these data: it amounts to approximately 25 vol.%, which agrees with the peak intensities on the diffractometer traces.

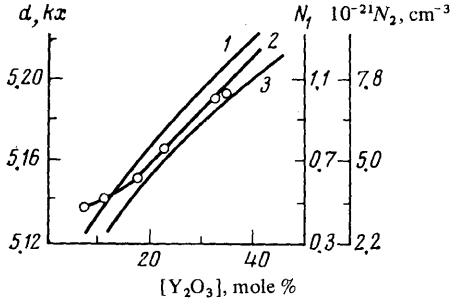


Figure 14. Variation of the lattice constant and of the number of vacancies in a ZrO_2–Y_2O_3 crystal as a function of the Y_2O_3 content: 1) lattice constant d calculated from Eqn. (2); 2) experimental values of d; 3) number of vacancies in the anionic sublattice (N_1—in the unit cell; N_2—in 1 cm^3).

The number of anionic vacancies V per unit cell was determined from the formula $V = 4m/(100 + m)$. The plot in Fig. 14*a* shows that each unit cell of the crystal with 33 mole % Y_2O_3 contains one O vacancy, which corresponds to 7.1×10^{21} in 1 cm^3. Fig. 15 presents curves characterising the degree of order in the structure. Evidently the degree of order is a maximum in the presence of 15 mole % Y_2O_3. With decrease of the Y_2O_3 concentration, the degree of order falls sharply owing to the incomplete stabilisation of the cubic structure. With increase of m above 20%, the order in the structure also breaks

down owing to the gradual rearrangement of the fluorite type lattice into the lattice of the solid solution of ZrO_2 in Y_2O_3.

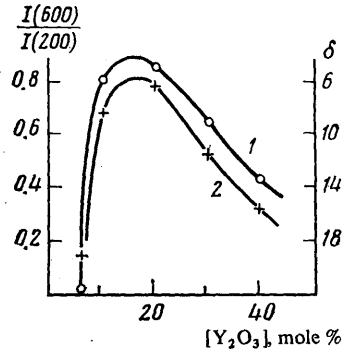


Figure 15. Variation of the degree of order as a function of the Y_2O_3 content: 1) width of (531) line at the level of half its height; 2) ratio of the intensities of the (600) and (200) lines.

Table 4. The densities of zirconium dioxide single crystals as a function of the concentration of the stabilising Y_2O_3 admixture (ρ_1 calculated from X-ray diffraction data and ρ_2 determined by hydrostatic weighing).

$[Y_2O_3]$, mole %	ρ_1, g cm^{-3}	ρ_2, g cm^{-3}	$[Y_2O_3]$, mole %	ρ_1, g cm^{-3}	ρ_2, g cm^{-3}
10.3	5.920	5.910	19.8	5.661	5.655
13.8	5.868	5.863	31.2	5.596	5.603
16.3	5.766	5.800	35.9	5.538	5.543

We calculated the densities of the single crystals from the X-ray diffraction data[39]. These results (ρ_1) together with the experimental values obtained by hydrostatic weighing (ρ_2)[40] are presented in Table 4. The appreciable decrease of the density of the crystals is caused both by the increase of the volume of the unit cell and by the increase of the concentration of the oxygen vacancies. Electron microscope studies, carried out using a "Stereoscan" raster microscope, confirmed that the specimens with 6 mole % Y_2O_3 consist of two phases. The photograph clearly shows inclusions having different structures and orientations. The structure of the crystals with 10–20 mole % Y_2O_3 is homogeneous. The X-ray diffraction data showed that the specimens with 30 mole % Y_2O_3 have a disordered single-phase structure. Nevertheless the electron micrographs showed patterns characteristic of two-phase systems. Presumably a phase having a Y_2O_3 concentration different from the average value, in which the given type of lattice is preserved with somewhat altered parameters, is segregated in these specimens.

Structural Substitutions and Point Defects

The results of the X-ray diffraction analysis and the density measurements showed that the stabilised ZrO_2 and HfO_2 crystals are substitutional solid solutions in which the cations of the stabilising oxide substitute Zr^{IV} ions (atoms). Since we are dealing here with heterovalent substitution, the formation of the solid solution is accompanied by the immediate appearance of several point defects. In terms of structural elements[41], the pattern has the following appearance.

(1) $Zr(Hf)O_2$–AO solid solutions, where A = Mg, Ca, Sr, or Ba. Here the structural elements are as follows: Zr_{Zr}—a zirconium ion in the cationic fluorite sublattice; A_{Zr}—a cation of the stabilising oxide at a site of the zirconium sublattice; V_O—a vacancy at an oxygen subsite of the fluorite sublattice; O_O—an oxygen ion at an anionic lattice site.

The concentrations of the structural elements are related as follows: when the mole fraction of AO in $Zr(Hf)O_2$ is n_1, the fraction of cationic sublattice sites occupied by the A ions is $[A_{Zr}] = n_1$ and the fraction of vacant anionic sublattice sites is $[V_O] = n_1$, which implies that each bivalent ion A introduces one oxygen vacancy.

(2) $Zr(Hf)O_2$–B_2O_3 solid solutions, where B = Sc, Y, La, or Ln. In this case the relative concentrations of the structural elements can be formulated thus: $[B_{Zr}] = 2n_2$; $[V_O] = n_2$; this implies that one oxygen vacancy is introduced by each two tervalent B ions.

Thus stabilisation by the addition of extraneous oxides introduces into the ZrO_2 and HfO_2 crystal lattices a large number of point defects, which greatly influence (as will be shown below) the physical properties of these crystals, particularly the electrical and spectroscopic properties.

Optical Inhomogeneity

The majority of the stabilised ZrO_2 and HfO_2 single crystals which we obtained exhibited a high degree of optical perfection. However, defects were encountered in certain specimens; we shall consider[42] the most typical of these. The optical inhomogeneity of a solid solution is known to be largely determined by the uniformity of the distribution of the solution components, which depends in its turn on the effective partition coefficient. We determined[42] the partition coefficient of Y_2O_3 in the ZrO_2–Y_2O_3 solid solution, and the effective partition coefficient was calculated by the method of Vigdorovich et al.[43] The Y_2O_3 concentration along the length of the crystal was determined by chemical analysis. In the presence of 10 mole% Y_2O_3, the partition coefficient is 1.088.[42]

The study of ZrO_2–Y_2O_3 and HfO_2–Y_2O_3 crystals under the microscope using crossed Nicol prisms revealed a weak inhomogeneity of the extinction caused by internal stresses. The angle between the optical axes was close to 90°. The difference between the refractive indices n_1 and n_2, obtained from the formula $\Delta\lambda = \alpha(n_1 - n_2)$ and a colour nomogram (for a plate thickness d = 1.5 mm), was 7.7×10^{-4}. Conoscopic studies showed that isotropic ZrO_2–Y_2O_3 and HfO_2–Y_2O_3 crystals become biaxial and optically positive under the influence of residual stresses, but the degree of deformation is small. The optical indicatrix of the crystals consists of a weakly deformed sphere, slightly extended in the direction of the [011] crystal growth axis. In order to eliminate internal stresses, the crystals were subjected to high-temperature

annealing *in vacuo* or in nitrogen. The rate of evaporation of the crystals at different temperatures was determined beforehand and it was found that appreciable evaporation begins at 2100° C. The rates of evaporation at this temperature were $(7-9)\times10^{-6}$ g cm^{-2} s^{-1} for ZrO_2–Y_2O_3 and $(3-5)\times10^{-6}$ g cm^{-2} s^{-1} for HfO_2–Y_2O_3 (the Y_2O_3 concentration was 10 mole % in both cases). These results showed that it is desirable to carry out the annealing at temperatures not exceeding 2100° C.

The dislocation structure was investigated by the chemical etching method. The most suitable etch is the $2HNO_3 + 3HF$ mixture. The typical density of dislocations in the [111] plane was 5×10^6 cm^{-2}. The etching pits were triangular in shape and were distributed extremely non-uniformly; their density increased markedly at the edges of the single crystal blocks. After annealing, the dislocation density decreased by an order of magnitude.

It has been noted that the crystals become black after annealing *in vacuo* (10^{-3} mmHg) at 2000° C with subsequent rapid cooling (at a rate of 450 K h^{-1}).[42] For low cooling rates, there was no blackening. When the blackened crystals were heated in air at 1200° C, their initial colour and transparency were restored. The blackening is associated with a partial loss of oxygen and the formation of colour centres, the retention of which on rapid cooling is due to the quenching of the reduced state of zirconium. During slow cooling, there is apparently sufficient time for a rearrangement of the lattice and the "reduced" zirconium is reoxidised by atmospheric oxygen.

One of the most characteristic forms of inhomogeneity in the crystals investigated consists of knotlike defects distributed at right angles to the direction of growth. They can be readily seen on shadow-projection patterns recorded by the shining point method[42]. The nature and distribution of the light-scattering particles were investigated using a laser ultramicroscope[42]; the observations were made at an angle of 90° to the direction of the incident beam from the He–Ne laser ($\lambda = 0.63$ μm). In certain ZrO_2–Y_2O_3 crystals with an additional admixture of erbium, cerium, and neodymium oxides, microscopic and submicroscopic particles with dimensions ranging from 0.03 to 8 μm were readily seen under the microscope. In highly defective specimens the average density of these particles reached $(0.5-1)\times10^6$ mm^{-3}. Under the influence of prolonged high-temperature vacuum annealing, the scattering particles increase in size and their number diminishes almost by a factor of 2. In ZrO_2–Y_2O_3 crystals without an additional admixture light scattering was observed in the form of a Tyndal cone, its intensity depending significantly on the purity of the initial substances and the conditions of crystal growth. Microscope studies showed that in this case the scattering is due to particles with dimensions of the order of 0.1 λ. The Y_2O_3 concentration does not affect the size and number of particles; on the other hand, the addition of a second admixture frequently resulted in the appearance of scattering centres.

Optical Properties

The first measurements of the refractive indices of stabilised ZrO_2 and HfO_2 single crystals were made by Aleksandrov et al.[40] In a later study[42] the refractive indices were measured on a precision goniometer by the prism method; the results of the measurements for ZrO_2–Y_2O_3 and HfO_2–Y_2O_3 are presented in Table 5, which also illustrates the dependence of the refractive index on the wavelength. It was noted[42] that the refractive index varies along the crystal length, the variation reaching several thousandths, which is due to the non-uniformity of the yttrium oxide concentration.

Table 5. The refractive indices n of zirconium dioxide single crystals as a function of yttrium oxide concentration (mole %).

λ, μm	Refractive index n			
	$[Y_2O_3]=9$	$[Y_2O_3]=11$	$[Y_2O_3]=15$	$[Y_2O_3]=17$
0.4358	2.2224	2.2101	2.1783	2.1232
0.5461	2.1856	2.1737	2.1434	2.0949
0.5779	2.1790	2.1669	2.1372	2.0897
0.5893	2.1768	2.1653	2.1352	2.0881
0.6328	2.1718	2.1581	2.1287	2.0826

Spectroscopic properties

A characteristic feature of the stabilised ZrO_2 and HfO_2 crystals is a large number of a wide variety of impurities at high concentrations, sometimes reaching 10 mole %. The phase homogeneity of the crystals is unaffected. Lanthanide elements, iron-group elements, chromium, vanadium, titanium, and many others can be introduced into these crystals. Many impurities can exist in several valence states in solid solutions based on ZrO_2 and HfO_2. In essence these solid solutions represent a whole class of substances, which, while retaining their macrostructure and phase homogeneity, can exhibit a variation in their physical properties within wide limits. We shall quote several examples of the spectroscopic properties of solid solutions based on ZrO_2 and HfO_2 with different impurities, illustrating the characteristics of these systems in relation to other impurity-containing crystals used in optics and quantum electronics.

1. Spectra of ZrO_2 and HfO_2 with an admixture of tervalent lanthanides. These crystals are of interest in view of the possibility of their employment in quantum electronics[44-46]. Fig. 16*a* illustrates the combined absorption spectrum of HfO_2–Y_2O_3–Nd_2O_3 (0.7 wt.%) at 300 K; Figs. 16*b* and 16*c* illustrate the absorption spectrum of Nd^{3+} ($^4I_{9/2} \rightarrow {}^4F_{3/2}$ transition) and the luminescence spectrum ($^4F_{3/2} \rightarrow {}^4I_{11/2}$ transition) of the same crystal, both recorded at 300 K on a DSF-12 spectrometer. The width of the Stark components of the spectra depends only slightly on temperature and amounts to 100 cm^{-1}. Analogous Nd^{3+} spectra were observed for ZrO_2–Y_2O_3–Nd_2O_3 crystals. The measured lifetime of the $Nd^{3+}(^4F_{3/2})$ level was 450 ± 30 μs in both cases. The lasing effect of Nd^{3+} in ZrO_2–Y_2O_3 and HfO_2–Y_2O_3 was investigated in an elliptical illuminator with an IFP-800 xenon pulse lamp. The resonator consisted of external dielectric mirrors with reflectivities of 99.9 and 97% for $\lambda = 1.06$ μm. A lasing effect was observed for ZrO_2–Y_2O_3–Nd_2O_3 crystals at a wavelength of 1.0609 μm and for HfO_2–Y_2O_3–Nd_2O_3 crystals at a wavelength of 1.0604 μm. The thresholds of the lasing effects of crystals between 24 and 32 mm long and between 3 and 6 mm in diameter were in the range 7–20 J. The widths of the laser lines were 34 and 38 Å respectively[44]. Thus, in terms of their spectroscopic and laser properties, the crystals of solid solutions based on ZrO_2 and HfO_2 occupy a position intermediate between crystals and glasses, exactly like other crystalline solid solutions

with a disordered structure. It has been noted[47] that the inhomogeneous broadening of the lines in the spectra of lanthanide ions in solid solutions is associated with the number of intrinsic and impurity point defects and increases with increase of the concentration of the impurities introduced.

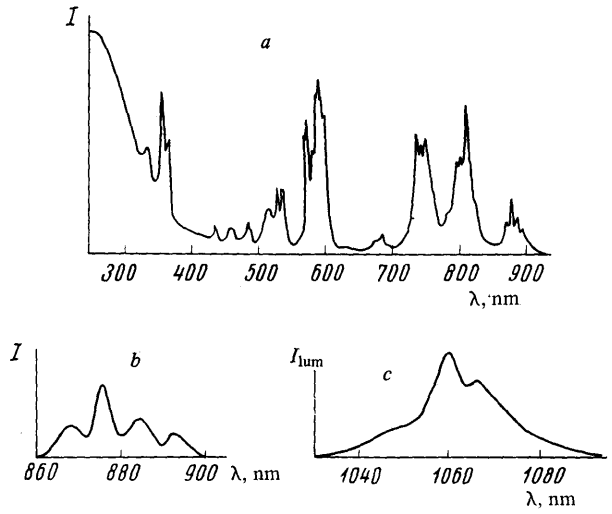


Figure 16. Optical spectra of HfO_2–Nd^{3+} crystals: *a*) absorption spectrum of HfO_2–Y_2O_3–Nd^{3+} (0.7 wt.%) crystals at 300 K: *b*) Nd^{3+} absorption band corresponding to the $^4I_{9/2} \rightarrow {}^4F_{3/2}$ transition; *c*) luminescence spectrum corresponding to the $^4F_{3/2} \rightarrow {}^4I_{11/2}$ transition at 300 K (*I* — line intensity).

The same characteristics of the spectra are typical also for ZrO_2–Er_2O_3–Ho_2O_3 and ZrO_2–Er_2O_3–TmO_3 crystals[46], which are of interest for lasers emitting in the region of wavelengths of approximately 2 μm. Here Er_2O_3 plays simultaneously the role of the stabiliser of the cubic structure and of the sensitiser of holmium and thulium. The lifetimes of the upper working $Ho^{3+}(^5I_7)$ and $Tm^{3+}(^3H_4)$ levels were 6.2 and 1.2 ms at 300 K and 6.6 and 2.5 ms at 77 K respectively. The lifetime of the $^4I_{13/2}$ level of the Er^{3+} ion without Ho^{3+} or Tm^{3+} admixtures was 8.5 ms. In the presence of Ho^{3+} and Tm^{3+} the luminescence of Er^{3+} originating from the $^4I_{13/2}$ level could not be recorded. The lasing effects of ZrO_2–ErO_3 (20 mole %)–Ho_2O_3 (1 mole %) and ZrO_2–Er_2O_3 (20 mole %)–Tm_2O_3 (1 mole %) crystals were observed in an elliptical illuminator with an IFP-2000 xenon pulse lamp. The laser crystals in the form of cylinders 33 mm long and 6.7 mm in diameter were placed in a quartz Dewar vessel with liquid nitrogen. Silver mirrors were deposited on the end-faces of the crystals; the reflection coefficients of the mirrors at the operational wavelengths were 100 and 95%. The lasing effect threshold amounted to 400 J for Ho^{3+} and 420 J for Tm^{3+}; the wavelengths of the lasing effects were 2.115 μm for Ho^{3+} and 1.896 μm for Tm^{3+}, which corresponds to the $^5I_7 \rightarrow {}^5I_8$ and $^3H_4 \rightarrow {}^3H_6$ transitions. For 800 J pumping, a lasing effect appeared in both crystals at λ = 1.620 μm. The results of the study of these crystals showed that they can find applications in redesigned lasers, since they have much narrower thresholds than glasses for a broad spontaneous emission spectrum.

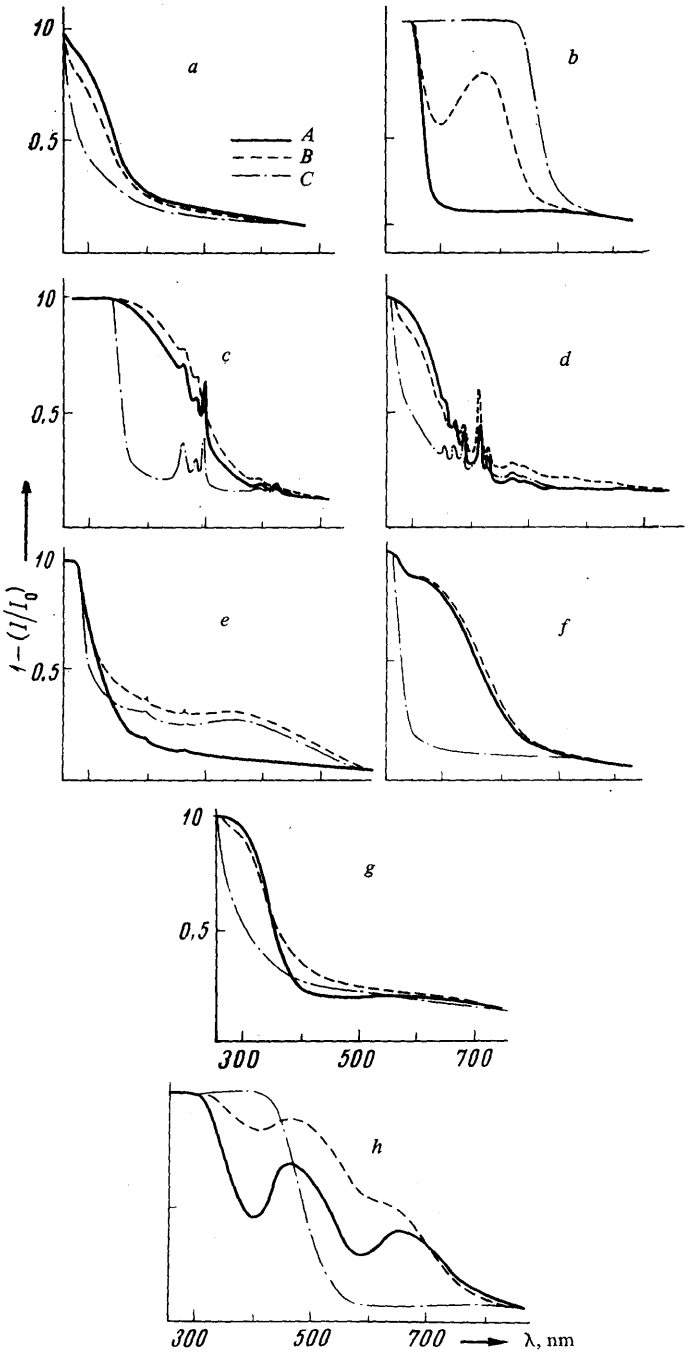


Figure 17. Absorption spectra of ZrO_2–Y_2O_3 crystals grown in air (*A*), after γ-irradiation (*B*), and after vacuum annealing (*C*): *a*) inactivated crystals with *d* = 5.47 mm; crystals activated by the addition of various lanthanides: *b*) Ce, *d* = 2.23 mm; *c*) Pr, *d* = 1.90 mm; *d*) Sm, *d* = 0.5 mm; *e*) Eu, *d* = 1.48 mm; *f*) Tb, *d* = 1.61 mm; *g*) Yb, *d* = 4.54 mm; *h*) Cr, *d* = 0.96 mm.

2. Spectroscopic properties of $Zr(Hf)O_2$–Y_2O_3 crystals with variable-valence impurity ions. In the study of crystals of solid solutions based on ZrO_2 and HfO_2 with impurities it was noted that their optical properties are sensitive to the oxidation-reduction heat treatment conditions and to the effect of ionising radiation. As a rule, these were crystals with admixtures of elements tending to undergo a change in their valence state. These results are of interest not only for spectroscopy but also from the standpoint of the structures of the crystals and the transformations of the structures of point defects. We shall quote data for ZrO_2–Y_2O_3 crystals activated by lanthanide and chromium ions[48]. The Ce, Pr, Sm, Eu, Tb, Yb, and Cr concentrations were 0.5 wt.%. The initial substances had the following purities: ZrO_2 was of "specially pure" grade, Y_2O_3 and lanthanide oxides were 99.999% pure, and chromium oxide was of "chemically pure" grade. The absorption spectra were recorded immediately after growing the crystals in air (spectra A) and then after each of the following types of treatment: (1) after exposure to ^{60}Co γ-rays at room temperature up to a dose of 10^7 rad (spectra B); (2) after vacuum annealing at 1800° C (spectra C). The spectra are presented in Fig. 17. They evidently vary as a function of the type of treatment of the crystals, the nature of the changes being related to the activator introduced. Only slight changes in the ultraviolet spectrum are observed for the inactivated crystals and crystals with samarium and ytterbium; the changes for the crystals activated with cerium, praseodymium, terbium, europium, or chromium are much more appreciable and they are accompanied by the appearance of new bands or disappearance of old ones in the visible part of the spectrum. The spectrum of the ZrO_2–Y_2O_3–Ce crystal, subjected to additional annealing in an oxidising atmosphere after vacuum annealing, agreed with that of the initial crystal (spectrum A). Heat treatment of γ-irradiated crystals results in the disappearance of bands induced by irradiation; γ-irradiation at 77 K made all the crystals opaque in the visible part of the spectrum. On subsequent heating to room temperature, they were gradually decolorised.

Spectra A

A striking feature of the absorption spectra of the crystals grown in air is the absence of Ce^{3+} bands from the spectrum of ZrO_2–Y_2O_3–Ce and the presence of an absorption band in the region of 3500–6000 K of the spectra of the Pr^{3+} and Tb^{3+} containing crystals together with the absorption bands due to Pr^{3+} and Tb^{3+}. An analogous band in the range 3000–5000 Å appears in the spectra of the γ-irradiated $Y_3Al_5O_{12}$–Pr and $Y_3Al_5O_{12}$–Tb crystals, where it is associated with the presence of Pr^{4+} and Tb^{4+} ions[49]. The tervalent Ce^{3+}, Pr^{3+}, and Tb^{3+} ions in the crystals are known to pass readily to the tervalent state[50]. Bearing this feature in mind as well as the oxidising conditions during crystal growth and the favourable conditions for the tetravalent state of the impurity in the ZrO_2 lattice, one may conclude that the entire cerium and part of the praseodymium and terbium are incorporated in the tetravalent state into the crystals of cubic ZrO_2 during the growth process. Under these conditions, admixtures of samarium, europium, ytterbium, and chromium are present as tervalent ions.

Spectra B

γ-Irradiation of crystals containing admixtures of cerium and europium in air leads to the appearance of new bands, compared with spectra A; these are the bands of the Ce^{3+} and Eu^{2+} ions. After irradiation of the crystals containing praseodymium and terbium, the intensity of the band at 3500–6000 Å increases slightly owing to the additional conversion of part of Pr^{3+} and Tb^{3+} into Pr^{4+} and Tb^{4+}. Spectrum B of the crystal with an admixture of chromium does not permit an unambiguous determination of the factor with which the increase of the intensities of the bands present in spectra A is associated. One may assume tentatively that the crystal grown in air contains Cr^{4+} together with Cr^{3+}. The increase of the band intensity can then be attributed to the conversion of Cr^{4+} into Cr^{3+} on γ-irradiation.

Spectra C

It follows from Fig. 17 that vacuum annealing has a strong influence on the absorption spectra of the crystals. The band in the range 2600–3700 Å disappears from the spectra of ZrO_2–Y_2O_3 crystals and crystals containing samarium and ytterbium; the 3500–6000 Å band disappears from the spectra of crystals with praseodymium and terbium, only the bands characteristic of the lanthanides remaining. By analogy with the $Y_3Al_5O_{12}$–Pr and $Y_3Al_5O_{12}$–Tb crystals the absorption band in the region from 3000 Å to the edge of the intrinsic absorption may be identified with the $4f \rightarrow 5d$ transitions in the Pr^{3+} and Tb^{3+} ions. As in spectra B, bands due to Ce^{3+} and Eu^{2+} appear in spectra C of ZrO_2–Y_2O_3–Ce and ZrO_2–Y_2O_3–Eu. A new band arises in the region of 4000 Å in the spectrum of the crystal with chromium and the Cr^{3+} bands vanish. All these changes indicate the reduction of activators during vacuum annealing, which is most likely to be associated with the formation of atomic oxygen during this process and its removal from the lattice. Repeated annealing in an oxidising atmosphere restores the original state of the specimens, i.e. the changes occurring on heating the specimens *in vacuo* to 1800° C lead to reversible changes in the nature and concentration of point defects. With increase of the temperature of the vacuum annealing, the changes become irreversible: the crystals blackened *in vacuo* remain turbid after heat treatment in air[42]. The results suggest that the disappearance of the Cr^{3+} bands after vacuum annealing indicates the conversion of Cr^{3+} into Cr^{2+}, while the decrease of the intensity of the 2600–3700 Å band in spectra B and its complete disappearance from spectra C of ZrO_2–Y_2O_3, ZrO_2–Y_2O_3–Sm, and ZrO_2–Y_2O_3–Yb crystals shows that the band is due to defects having an effective positive charge and containing a captured electron—most probably oxygen vacancies.

Thus the formation of colour centres in the activated crystals of cubic ZrO_2–Y_2O_3 solid solutions on γ-irradiation and heat treatment is associated mainly with the capture of charge carriers by activator centres and is determined by their nature. The relatively high radiation stability of ZrO_2–Y_2O_3 crystals at room temperature is due to the small depth of the majority of "intrinsic" capture levels in the forbidden gap.

Electrical Properties

It has been established[51] that the ionic type of conductivity predominates in the ZrO_2 ceramics stabilised by CaO, SrO, Y_2O_3, and La_2O_3. Data have been published[52] for the conductivities of polycrystalline zirconium and hafnium dioxide specimens in the temperature range 500–1300° C. Fig. 18 illustrates the temperature dependence of the resistivities of ZrO_2–Y_2O_3 (10 mole %) and HfO_2–Y_2O_3 (10 mole %) single crystals, obtained by the three-probe method[53]. At low temperatures the experimental points lie on curves described by the equation $\rho = 1.6 \times 10^{-4} \exp(1.20/kT)$ for HfO_2–Y_2O_3 (10 mole %) and $\rho = 3.1 \times 10^{-5} \exp(1.12/kT)$ for ZrO_2–Y_2O_3 (10 mole %), where kT is expressed in eV and ρ in Ω cm. The resistivities of various specimens of ZrO_2–Y_2O_3 single crystals having the same nominal compositions differed appreciably in the low temperature region, apparently owing to the different concentrations of defects in the crystals grown under different conditions. If an electric field is applied to a crystal heated to 300° C and above, then a coloured region arises at the negative electrode, which then begins to grow towards the anode. A broad band appears in the absorption spectrum near the intrinsic absorption edge (of the kind obtained after γ-irradiation of the crystals); it can be fairly justifiably assigned to oxygen vacancies which have captured electrons.

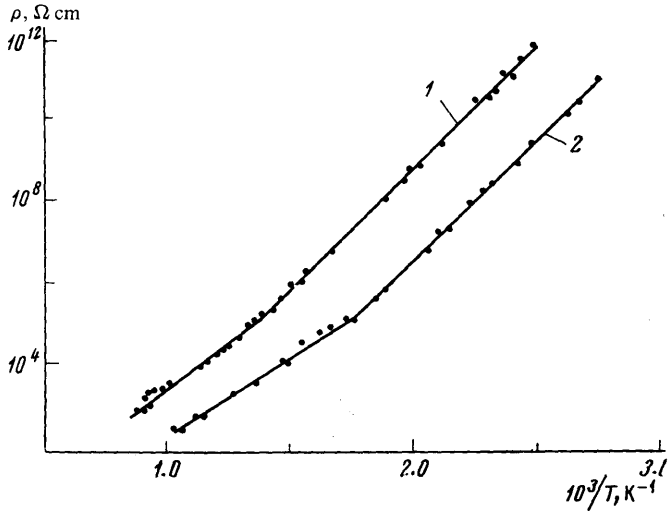


Figure 18. Temperature variation of the resistivity of single crystals: 1) HfO_2–Y_2O_3 (10 mole %); 2) ZrO_2–Y_2O_3 (10 mole %).

Fig. 19 presents the frequency dependence of $\epsilon \tan\delta$ for ZrO_2–Y_2O_3 (10 mole %) and HfO_2–Y_2O_3 (10 mole %), while Fig. 20 shows the temperature dependence of ϵ and $\tan\delta$.[53] The relatively small variance of ϵ shows that the polarisation of the crystals investigated has a relaxation mechanism and may be caused by the displacement of weakly bound oxygen vacancies or impurity ions. Fig. 20 shows that ϵ increases with temperature.

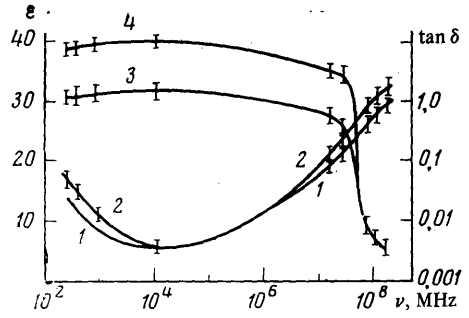


Figure 19. Frequency dependence of ϵ and $\tan\delta$ for HfO_2–Y_2O_3 (10 mole %) single crystals [1) $\tan\delta$; 3) ϵ] and ZrO_2–Y_2O_3 (10 mole %) single crystals [2) $\tan\delta$; 4) ϵ].

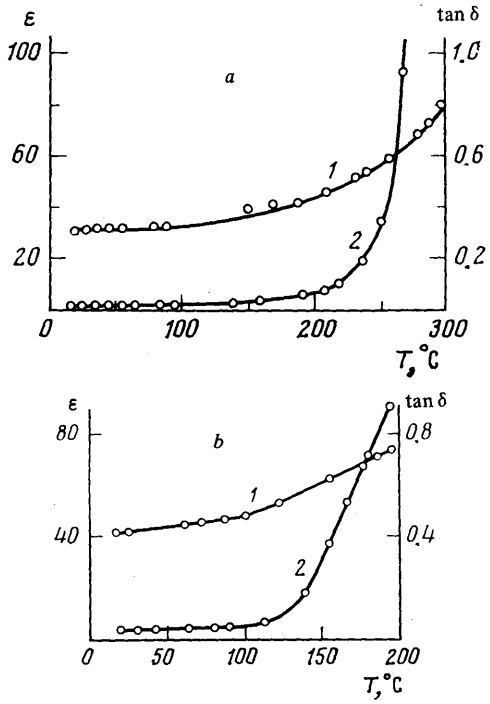


Figure 20. Temperature dependence of ϵ and $\tan\delta$ for different single crystals: *a*) HfO_2–Y_2O_3 (10 mole %); *b*) ZrO_2–Y_2O_3 (10 mole %); 1) ϵ; 2) $\tan\delta$.

The electrical conductivities of zirconium dioxide single crystals have been investigated[54] at temperatures between 800° and 1900° C. The measurements were performed either in a tubular graphite furnace in a vacuum of 0.1 mmHg or in an inert atmosphere by the four-probe method using 50 Hz a.c. on the apparatus already described[55]. The electrical conductivity was measured both with a gradual increase of temperature from 800° to 1900° C and with subsequent stepwise cooling[54]. This made it possible to take into account the influence of the defects associated with the partial reduction of the crystals. Comparison of data for single crystals and ceramic specimens having the same composition showed that the single crystals have a

specific conductance greater by a factor of 1.5. Fig. 21 presents data for ternary systems containing 10 mole % of the stabilising impurity and 1 wt.% of one of the lanthanide oxides. Evidently, after the addition of the second admixture, the electrical conductivity increases. It initially rises from cerium to praseodymium and then falls for neodymium and again rises from neodymium to terbium.

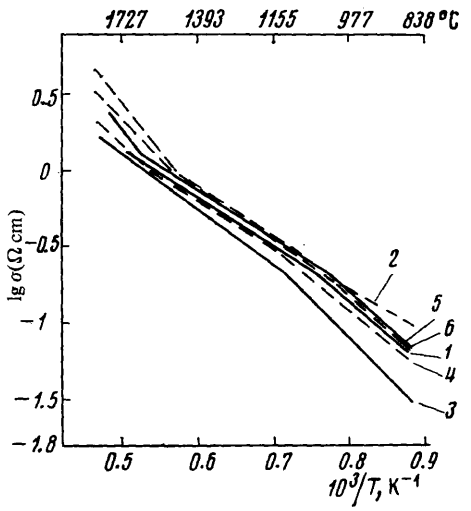


Figure 21. Temperature dependence of the resistivities of single crystals: 1) ZrO_2–Y_2O_3 (10 mole %) + 1 wt.% CeO_2; 2) ZrO_2–Y_2O_3 (10 mole %) + 1 wt.% Pr_6O_{11}; 3) ZrO_2–Y_2O_3 (10 mole %) + 1 wt.% Nd_2O_3; 4) ZrO_2–Y_2O_3 (10 mole %) + 1 wt.% Sm_2O_3; 5) ZrO_2–Y_2O_3 (10 mole %) + 1 wt.% Tb_2O_3; 6) ZrO_2–Y_2O_3 (10 mole %) + 1 wt.% Yb_2O_3.

Elastic, Photoelastic, and Acoustic Parameters

The elastic, photoelastic, and acoustic properties of ZrO_2–Y_2O_3 and HfO_2–Y_2O_3 single crystals have been measured[56–58] by the method of Mandelstam–Brillouin light scattering. The studies were performed on the experimental apparatus already described[59]. An Ar^+ laser served as the source of light at a wavelength of 5145 Å. The scattered light spectrum was investigated with the aid of a Fabry–Perot étalon, scanned as a function of pressure, and was recorded photoelectrically using a photon counting technique. The results of the data interpretation are presented in Tables 6–8. Analysis of the results led to the following findings:

1. In ZrO_2–Y_2O_3 and HfO_2–Y_2O_3 solid solutions there are directions of excited and scattered light for which longitudinal waves hardly contribute to light scattering. Analogous results had been obtained previously for non-cubic sapphire[61] and lithium niobate crystals[62].

2. The velocities of the longitudinal and transverse sound waves in ZrO_2–Y_2O_3 solid solutions depend significantly on the direction of their propagation, i.e. these cubic single crystals are strongly anisotropic with respect to the velocity of sound.

3. The constants C_{11} and C_{44} vary monotonically with the Y_2O_3 concentration, while C_{12} varies non-monotonically.

4. The elastic anisotropy of ZrO_2–Y_2O_3 crystals is very considerable and varies from 2 to 2.6 depending on the Y_2O_3 content. It follows from Table 7 that the photoelastic anisotropy of these crystals is just as great. It increases from 1.80 to 2.85 with increasing Y_2O_3 concentration.

Table 6. Acoustic parameters of ZrO_2–Y_2O_3 single crystals.

$[Y_2O_3]$, mole %	ρ, g cm^{-3}	Direction of propagation of sound	Polarisation of sound	Velocity of sound, km s^{-1}		Elastic constants x 10^{12}, dyn cm^{-2}			Debye temp., K
				Ref.57	Ref.60	C_{11}	C_{44}	C_{12}	
8	5.99	[110[	[001]	—	3.05	—	—	—	—
		[110]	[1$\bar{1}$0]	—	5.02	3.94	0.56	0.91	543
		[110]	[110]	—	7.05	—	—	—	—
10.3	5.91	[100]	[001]	3.12	—	—	—	—	—
		[100]	[100]	8.26	—	—	—	—	—
		[1/2—1/2, $\sqrt{1/2}$]	T_1	4.54	—	4.03	0 58	0.83	555
		[1/2—1/2, $\sqrt{1/2}$]	T_2	—	—	—	—	—	—
		[1/2—1/2, $\sqrt{1/2}$]	L	6.89	—	—	—	—	—
12	5.89	[110]	[001]	—	3.24	—	—	—	—
		[110]	[1$\bar{1}$0]	—	5.78	4.49	0.62	0.55	584
		[110]	[110]	—	7.30	—	—	—	—

Table 7. Elastic and photoelastic properties of ZrO_2–Y_2O_3 single crystals.

$[Y_2O_3]$, mole %	ρ, g cm^{-3}	Elastic anisotropy $(C_{11}-C_{12})/2C_{44}$	n	Photoelastic constants*			Anisotropy $(P_{11}-P_{12})/2P_4$
				P_{11}	P_{12}	P_{44}^*	
10	5.95	2.401	2.193	—	—	—	1.80
12	5.89	2.559	2.183	0.285	—0.115	0.100	2.00
16.5	5.81	2.347	2.177	—	—	—	2.63
20	5.76	2.001	2 174	0.470	—0.101	0.100	2.85

*It was arbitrarily assumed that the constant $P_{44} = 0.100$.

By virtue of a unique combination of their physical and physicochemical properties, fianit single crystals may be used in optics, high-temperature engineering, quantum electronics, and in the manufacture of jewellery. Fig. 22 presents photographs of technical articles (lenses, prisms, windows, crucibles, laser elements, and electrodes) made of fianits.

VI. PREPARATION OF HIGH-TEMPERATURE GLASSES

The glasses are usually prepared in gas or electrical furnaces in platinum or ceramic crucibles[63]. The same problems then arise as in the growing of crystals from the melt: (1) the difficulty of obtaining a product uncontaminated by the material of the crucible and (2) the difficulty of obtaining glasses at temperatures above 1600–1700° C. The first experiments on the preparation of glasses in a cold container were described by Aleksandrov et al.[14] and a later report[64] dealt with the preparation of glasses in quartz beakers exposed to a stream of gas with direct heating of the glass mass by high-frequency currents.

Certain properties of new high-temperature R_2O_3–Al_2O_3–SiO_2 glasses, where R_2O_3 = scandium, yttrium, or lanthanum oxide or the oxide of another lanthanide, are described below[65]. The preparation of glasses in a cold container has characteristic features distinguishing it from the preparation of crystals. In the first place the glasses do not have a distinct melting point and there is therefore also no distinct interface between the melt and the solid phase. The transition from the solid substance adjoining the walls of the cold container to the melt is gradual via a vitreous substance with a gradually diminishing viscosity. Another characteristic feature is the high viscosity of the glass melt, which hinders convection, mixing of the components, the removal of the glasses, and ultimately the homogenisation of the melt and the formation of a glass of a high optical quality. Fig. 23 presents a scheme for the preparation of high-temperature optically homogeneous glasses. We used a cooled stirrer in order to agitate the viscous melt. A crust of solid glass grows on the part of the stirrer immersed in the melt, so that stirring does not result in the contamination of the material.

Table 8. Velocity of sound in HfO_2–Y_2O_3 (10 mole %) {direction of exciting light [110]}.

Direction of scattered light	Wave*	Velocity of sound, km s^{-1}
$[\bar{1}10]$	L	6.29±0.04
$[1\bar{1}0]$	T_2	2.50±0.02
[001]	qL	5.46±0.02
[001]	T_2	3.20±0.01
[001]	qT_1	3.48±0.04

*Notation: L = longitudinal sound wave; T_2 = transverse sound wave with the direction of polarisation at right angles to the scattering plane; T_1 = ditto with the direction parallel to the scattering plane. The prefix q indicates that the sound wave is quasi-longitudinal or quasi-transverse.

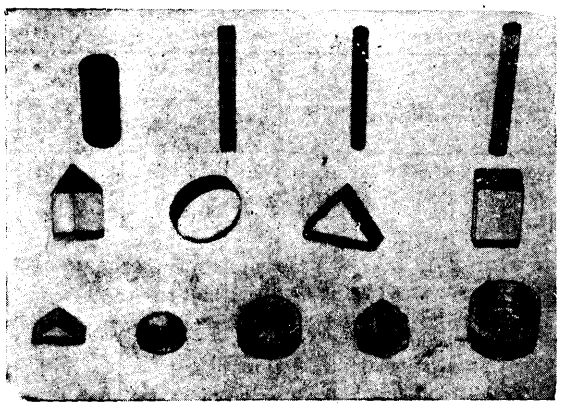


Figure 22. Photograph of technical articles made of fianits.

The glass was prepared over a period of several hours. The melt in the container was then cooled to 800° C and the resulting block was removed from the container and transferred to a Silit furnace for annealing (at 800° C), which was continued for 8 h. In order to obtain specimens of specified shape, the glass melt was poured into graphite boats. Glass blocks weighing up to 1.5 kg each were thus prepared. The glasses were optically homogeneous and did not contain bubbles or sections which had not been fused. Small bubbles were present only in a narrow region of the viscous melt adjoining the walls of the container.

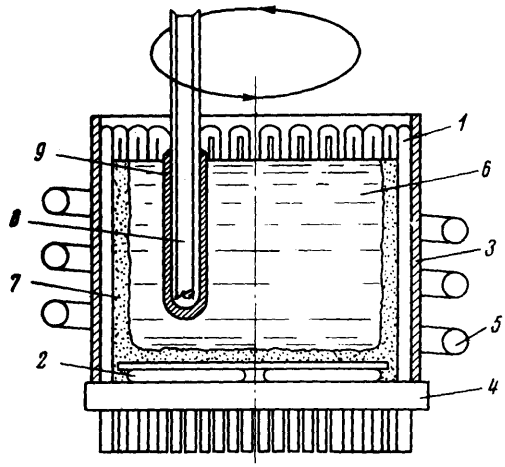


Figure 23. Scheme for the preparation of high-temperature glasses in a cold container: 1) tubular water-cooled element; 2) water-cooled bottom; 3) insulating quartz cylinder; 4) retaining ring of electrically insulating material; 5) inductor of high-frequency generator; 6) melt; 7) charge; 8) water-cooled stirrer; 9) garnissage.

Physicochemical Properties

The softening temperature of the metasilicate section through the Y_2O_3–Al_2O_3–SiO_2 system is in the range 1100–1300° C and increases with decrease of the Y_2O_3 concentration[65]. Analogous data were obtained also for scandium, lanthanum, and erbium glasses. The nature of the dilatometric curves for glasses with small amounts of added R_2O_3 is of interest (2–10 wt.%). Up to 1000° C normal thermal expansion of the glasses is observed, at 1000–1050° C the specimens undergo a sharp contraction, which terminates just as abruptly on further increase of temperature, and softening begins only above 1300° C (Fig. 24). An exothermic effect on the differential thermograms corresponds to the termination of the primary contraction (at 1000–1050° C) and an endothermic effect corresponds to the onset of softening. The exothermic peak is higher the smaller the content of the oxide R_2O_3. This effect is associated with the crystallisation of the glass. X-Ray and micro-X-ray spectroscopic studies on the specimens showed that, when glasses with small amounts of added R_2O_3 crystallise, the mullite phase ($3Al_2O_3.2SiO_2$) is produced. With increase of the R_2O_3 content, crystals of tervalent metal silicates or aluminosilicates begin to be

formed. Glasses containing Sc_2O_3 and La_2O_3 exhibit the highest and lowest capacities for crystallisation respectively, which is due to the difference between the basic properties of the oxides.

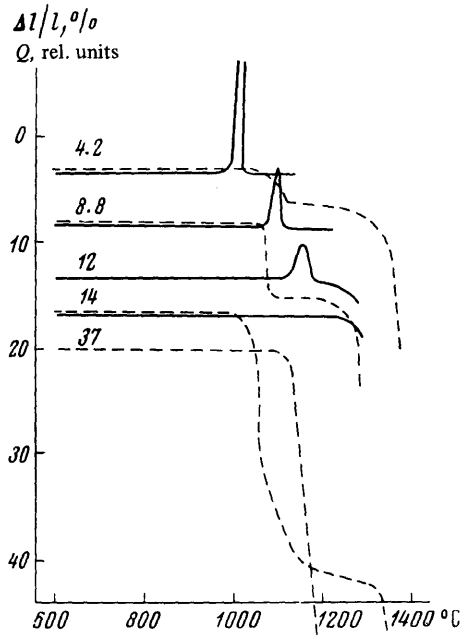


Figure 24. Dilatometric curves (shown dashed) and differential thermograms (shown continuous) for Er_2O_3–Al_2O_3–SiO_2 glasses (the numbers against the curves represent molar percentages of Er_2O_3). The origins of coordinates for the $\Delta l/l$ curve have been displaced along the ordinates axis relative to the upper curve.

Physicochemical and Electrical Properties

Table 9 presents the properties of certain high-temperature glasses obtained in a cold container[65]; the corresponding properties of quartz glass are included for comparison[66]. Evidently the mechanical properties of the glasses are similar to or somewhat superior to those of fused quartz, the softening temperatures of the glasses approaching that of quartz, while their refractive indices are higher than that of quartz. In contrast to the quartz glass, it is easy to introduce various admixtures, including lanthanides, into the glasses.

VII. THE PREPARATION AND PROPERTIES OF FUSED POLYCRYSTALLINE CERAMIC MATERIALS

The preparation of fused polycrystalline materials, used to make cast or pressed ceramic articles, differs little in principle from the process described above, which occurs in the course of high-temperature chemical reactions or when the crystals and glasses are synthesised. The melt having the required composition, prepared by the method described above, is kept for some time in the superheated state for homogenisation and then cooled rapidly. This results in the mass crystallisation of the melt and the latter sets in its entirety into a polycrystalline ingot consisting of fairly large crystalline grains. The fusion is usually carried out in containers having the design illustrated in Fig. 6*a*. Containers shown in Fig. 6*c* are used for the continuous fusion of the polycrystalline ingot.

Table 9. Physicomechanical and electrical properties of high-temperature glasses.

Property	Composition of glass, wt.%				
	quartz glass	SiO_2:Al_2O_3:Sc_2O_3=60:30:10	SiO_2:Al_2O_3:Y_2O_3=50:20:30	SiO_2:Al_2O_3:La_2O_3=54:21:25	SiO_2:Al_2O_3:Er_2O_3=60:30:10
Density, g cm^{-3}	2.20—2.21	2.578	3.05	3.016	2.833
Refractive index	1.4588	1.542	1.592	1.573	1.555
Young's modulus, kg mm^{-2}	7450—7140	12 740	11 040	9650	9080
Shear modulus, kg mm^{-2}	3200	5 100	4510	3940	3660
Poisson coefficient	0.16	0.249	0.225	0.225	0.240
Microhardness, kg mm^{-2}	795	780	1050	735	930
Coefficient of linear expansion, K^{-1}	$5\div7\cdot10^{-7}$	$27\cdot10^{-7}$	$70\cdot10^{-7}$	$28\cdot10^{-7}$	$10.3\cdot10^{-7}$
Temperature of onset of softening, °C	1250	1200—1250	1000	1100—1200	1150—1200
Resistivity, Ω cm					
at 20°C	$1\cdot10^{19}$—$1\cdot10^{18}$	$3\cdot10^{13}$	$2\cdot10^{13}$	$4\cdot10^{13}$	$1\cdot10^{13}$
at 600°C	$6\cdot10^{7}$—$6\cdot10^{6}$	$1.7\cdot10^{5}$	—	$1\cdot10^{5}$	$1.7\cdot10^{7}$
at 1000°C	$1\cdot10^{6}$—$2.5\cdot10^{5}$	$1.1\cdot10^{4}$	—	$5\cdot10^{3}$	$5\cdot10^{3}$
Dielectric constant at 20°C	3.2	6.8	7.0	7.1	6.9
Tangent of the dielectric loss angle in the frequency range 30 kHz–10 MHz	$2\cdot10^{-4}$	$5\cdot10^{-4}$	$2\cdot10^{-4}$	$1\cdot10^{-4}$	$2\cdot10^{-4}$

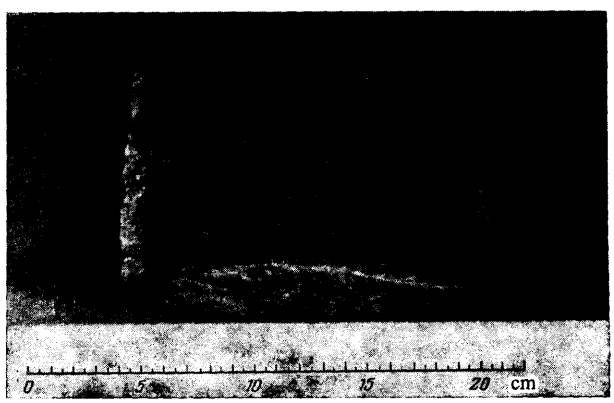


Figure 25. Photograph of a polycrystalline yttrium oxide ingot.

As an example, Fig. 25 presents a photograph of an yttrium oxide ingot. Its structure, indicating the form of the crystallisation isotherm, is clearly seen. We are in essence dealing here with directed crystallisation, since, even after the instantaneous switching off of the high-frequency generator, the large mass of the melt cools non-uniformly (faster at the water-cooled walls than in the centre), as a result of which a temperature gradient is

established in the bulk of the melt. Furthermore, a very large number of crystal nuclei, on which crystallisation takes place, are present at the walls of the solid shell. There are no nuclei in the central part of the melt and the onset of nucleation and crystal growth requires some supercooling. Nevertheless, even under these temperature conditions, some materials crystallise in the bulk phase, simultaneously in all parts of the melt. Yttrium chromite and yttrium aluminium garnet melts crystallise in this way (in air). As a result, ingots of these materials do not consist of large elongated blocks but comprise small isometric crystals. The nature of the crystallisation of the melt (directed or bulk phase) determines the homogeneity of the chemical and phase compositions of the ingot. This applies particularly to incongruent crystallisation and especially to the crystallisation of melts having a complex composition.



Figure 26. Electron micrograph of an $LaCrO_3$ ingot to which 7 mole % of calcium chromite has been added.

The Preparation and Properties of Electrically Conducting Fused Oxide Ceramic Materials

Oxide ceramic materials exhibiting ionic or electronic conduction have recently become important in connection with the development of high-temperature technology. Among the technical problems requiring the use of such materials, mention may be made of the formation of heating elements for furnaces giving temperatures up to 2000° C in an oxidising medium, the formation of the electrode walls of magnetohydrodynamic generators, and the development of sensors of the composition of the atmosphere at high temperatures. The manufacture of ceramic partitions with ionic conduction for new chemical current sources also represents an important problem. A new type of conducting material—lanthanum and lanthanide chromites having the general formula $RCrO_3$ and containing an admixture of calcium chromite—was proposed in 1960.[67] Later these materials were investigated[68-71] and it was found that they exhibit electronic conduction, the conductivity being fairly high even at room temperature.

A method has been developed for the synthesis and crystallisation of scandium, yttrium, lanthanum, and lanthanide chromites from the melt in a cold container[13,15]. The chromites obtained from the melt have a well-formed crystal structure and a high chemical purity and phase homogeneity. Certain properties of the fused chromites and the ceramics based on them are given below. Fig. 26 presents electron micrographs of the cleavage plane of the $LaCrO_3$ ingot containing an admixture of 7% of calcium chromite. The photographs clearly show crystalline grains of the lanthanum–calcium chromite solid solution and drops of the eutectic composition enriched (as shown by the X-ray microspectroscopic analysis) in calcium oxide, displaced to the boundaries between the crystals. The chromite ingots were ground and ceramic articles were made from the resulting powder by various procedures of ceramic technology.

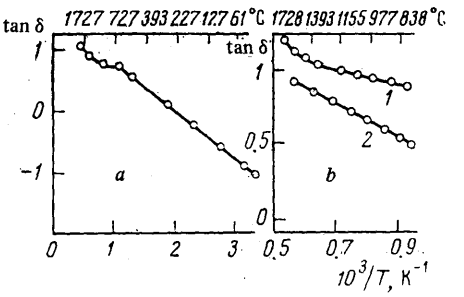


Figure 27. Temperature dependence of the electrical conductivity of a lanthanum chromite specimen to which 7 mole % of calcium chromite has been added: *a*) directly after preparation; *b*) heating in air (curve *1*) and cooling in argon (curve *2*).

Fig. 27 illustrates the temperature variation of the specific conductance of the ceramic made from fused lanthanum chromite with an admixture of calcium†. This material exhibits a high electrical conductivity even at room temperature. An interesting feature of the chromite ceramic is the marked dependence of its electrical conductivity on the oxidation-reduction properties of the atmosphere. A high conductivity in the temperature range between room temperature and 1000° C is ensured only after heat treatment of the specimens in an oxidising atmosphere. Heat treatment in a reducing or a neutral atmosphere or *in vacuo* sharply increases the resistivity of the ceramic in the low-temperature region (Fig. 27). Reheating in an oxidising atmosphere fully restores the initial conductivity. X-Ray diffraction studies on melted lanthanum chromite showed that the material subjected to reductive annealing contains only one phase ($LaCrO_3$). After heat treatment in an oxidising medium, the X-ray diffraction patterns show, together with the lines of the above phase, new lines indicating the appearance of an admixture of a new phase. Thus one may conclude that the electronic conductivity below 1000° C is associated with the formation in the material of admixtures in which the valence of chromium is higher than 3. The melted chromites obtained readily

† The conductivity data for the lanthanum and yttrium chromite ceramics were obtained by E. G. Spiridonov and V. G. Gordon at the High Temperature Institute (IVTAN).

combine with other metallic and non-metallic phases, initiating a new series of multiphase materials.

One of the most attractive ceramic materials for the manufacture of components with ionic low-temperature conduction for new current sources is Na-β-alumina having the composition $Na_2O.11Al_2O_3$.[72,73] By virtue of the characteristic features of the crystal structure of this compound, Na^+ ions are highly mobile even at 300° C, which makes it possible to employ the Na-β-alumina ceramic for partitions in sodium–sulphur accumulators. This compound is usually synthesised by sintering the initial components (Na_2CO_3 and Al_2O_3) below the melting point (m.p. 1930° C)[73,74]. It is then difficult to drive the reaction to completion and to ensure the absence of admixtures of non-conducting phases which increase the electrical resistivity of the product. Na-β-alumina has been synthesised and crystallised in the melt using the technique of direct high-frequency fusion in a cold container[74]. The starting materials were Al_2O_3 and Na_2CO_3 with a high degree of purity. The components were mixed and heat-treated for 2 h at 1000° C in order to remove the bulk of CO_2. After this the mixture, which had partly interacted, was transferred to a cold container and fused. The starting metal was aluminium. After the fusion of the material, the melt was maintained for 10–20 min at ~ 1980° C, whereupon the components reacted fully and the melt was homogenised. The power supplied to the melt was then gradually reduced and crystallisation was carried out. Single crystals grew on the surface of the melt in the form of square planar plates, the size of the sides of which reached up to 20 mm. The entire ingot was found to consist of fine crystalline blocks. The ingots were ground and ceramic articles were made from the powder. The densities of the specimens obtained were in the range 3.17–3.19 g cm^{-3} and the resistivities, measured using 150 kHz a.c. at 300° C, were 3–10 Ω cm.

If impurities are introduced to synthesise electrically conducting materials (we have in mind non-metals), then the electrically insulating materials must exhibit a high degree of chemical purity and structural perfection. In this respect the technique under consideration has many possibilities. A number of high-temperature insulating materials have been obtained: calcium and strontium zirconates and hafnates and yttrium, scandium, etc. oxides[15]. They all exhibit a high chemical purity, phase homogeneity, structural perfection and as a result have effective electrically insulating properties up to 2000° C. Owing to their high melting points, it is difficult to obtain these materials with a high purity, excluding the possibility of impurity conductivity, by other methods.

Another class of substances with interesting "electrical" properties, which are successfully obtained by crystallisation in a cold container, are dielectrics of the type of lanthanide titanates and zirconates (Table 3).[75]

The Preparation and Properties of Fused Materials for Refractory Ceramics

Refractory polycrystalline ceramics are widely used in metallurgy, chemistry, and high-temperature technology. The main requirements which must be met by such ceramics is high thermal stability and chemical stability at high temperatures. Both these properties are closely related to the chemical purity and structural perfection of the material of the ceramic. The use of the method of direct high-frequency fusion in a cold container[15] led to the preparation of fused polycrystalline ingots of many refractory materials: mullite, yttrium, scandium, and certain lanthanide oxides, spinels, zirconates, ternary aluminium, zirconium, and silicon oxide compounds (bakor) and certain silicates (Tables 2 and 3). Several examples are given below.

1. Mullite[76–78]. By virtue of its excellent thermal stability, this compound, which melts at 1910° C, is one of the most effective refractory materials. It is usually synthesised by the method of solid-phase reactions, which is time consuming and yields a product contaminated by the phases of the unreacted components. The mullite ingot obtained by crystallising the melt in a cold container consists of long prismatic needles oriented in the direction of crystallisation of the ingot. Analysis of the ingots showed that the crystalline phase in any part of the ingot has a composition differing from that of the individual compounds $3Al_2O_3.2SiO_2$ and $2Al_2O_3.SiO_2$ and corresponds to an intermediate composition in the region of a continuous series of solid solutions[76,77]. Table 10 presents certain properties of the ceramics obtained from fused mullite.

Table 10. The properties of ceramics based on materials obtained by direct high-frequency fusion in a cold container.

Property	Composition				
	$3Al_2O_3.2SiO_2$	Sc_2O_3	Y_2O_3	Gd_2O_3	Er_2O_3
Purity, %	99.7	99.0	99.9	99.98	99.9
M.p., °C	1970	2405	2410	2330	2340
True density, g cm^{-3}	3.15	3.96	5.03	8.33	8.66
Apparent density, g cm^{-3}	2.5—2.6	3.28	4.25	6.8	7.5
Apparent porosity, %	17—18	15—19	14.8	18.4	15.5
Ultimate compressive strength, kg cm^{-2}	500	1400	190	300—350	300—350
Ultimate bending strength, kg cm^{-2}					
at 20°C	150	—	120	—	—
at 1000°C	—	—	100	100—200	100—200
at 1300°C	—	—	125	—	—
at 1400°C	—	—	—	20	20
Modulus of elasticity 10^6E, kg cm^{-1}	0.37	—	1.5	—	—
Temperature of deformation under 2 kg cm^{-2} load, °C					
onset of softening	1760—1810	—	1950	—	—
4% contraction	1780—1830	—	2250	1700—1800	1700—1800
Creep *in vacuo*, mm mm^{-1} h^{-1}	—	—	—	—	—
at 1650°C, 14.7 kg cm^{-2} load	—	—	$9.8\cdot10^{-4}$	—	—
Coefficient of linear expansion, K^{-1}					
at 20–800°C	—	—	$7.3\cdot10^{-6}$	$8.4\cdot10^{-6}$	$7.5\cdot10^{-6}$
at 850°C	$4.4\cdot10^{-6}$	—	—	—	—
Resistivity, Ω cm					
in vacuo at 1000°C	—	—	$2.5\cdot10^{8}$	—	—
in vacuo at 1500°C	—	—	$3.0\cdot10^{3}$	—	—
in air at 1000°C	—	—	$1\cdot10^{9}$	10^4—10^5	—
in air at 1600°C	—	—	$3\cdot10^{8}$	—	—
Thermal conductivity at 1200°C, kcal m^{-1} h^{-1} K^{-1}	—	—	0.75	—	—
Thermal stability at 1300°C in water	—	—	12	—	—
Rate of evaporation *in vacuo*, g cm^{-2} s^{-1}					
at 1700°C	$0.5\cdot10^{-7}$	—	—	—	—
at 1800°C	$1.0\cdot10^{-7}$	—	—	—	—
at 1900 °C	—	—	$1.6\cdot10^{-5}$	$6.0\cdot10^{-5}$	$1.2\cdot10^{-5}$
at 2000°C	—	—	$1.5\cdot10^{-7}$	$2.0\cdot10^{-4}$	$1.9\cdot10^{-5}$

2. Y_2O_3, Gd_2O_3, Er_2O_3, and Sc_2O_3.[79–83] The dense polycrystalline yttrium oxide ceramic is highly refractory, has effective dielectric and mechanical properties, and is involatile. We used yttrium oxide of type Y–O with an overall impurity content of ~ 0.1% for fusion

and crystallisation[82]. The fusion process was initiated with metallic yttrium having the corresponding purity. In order to obtain an ingot consisting of large crystals, after heat treatment for 15–20 min the container with the melt was lowered at a rate of 100–200 mm h^{-1} relative to the inductor, which resulted in directed crystallisation of the melt. The ingot obtained was colourless on the outside, but after cleavage it was seen that its internal regions were intensely coloured greyish-blue. After annealing in air at 1200°C, the colour disappeared. These findings showed that, even on fusion in air, yttrium oxide is partly reduced, which leads to the formation of colour centres. As the outer parts of the material in contact with the oxidising atmosphere are cooled, the previously reduced yttrium is reoxidised to the tervalent state. Fig. 25 presents a photograph of an yttrium oxide ingot consisting of large crystals. A granular ceramic material was obtained from fused Y_2O_3 by pressing using a liquid binder; some of its properties are presented in Table 10.

Fused polycrystalline gadolinium, erbium, and scandium oxides are extremely promising as high-temperature constructional materials. The preparation of these substances does not differ in principle from the preparation of crystalline yttrium oxide. Some of the properties of the granular ceramics obtained from fused Sc_2O_3, Gd_2O_3, and Er_2O_3 [81-83] are presented in Table 10.

---o0o---

Examination of the possibilities of the new technology and the study of the properties of the materials obtained with its aid permit the following conclusions.

Direct high-frequency fusion in a cold container has major technological advantages. For example, it is possible to obtain with the aid of this technique multiphase eutectic compositions and structured compound materials of the metal–oxide and oxide–oxide types by direct fusion and crystallisation of the melt in a cold container as well as new glasses, single crystals, and single-phase ceramic materials, some of which were described above.

By virtue of its fundamental advantages and the ease of its practical application, the method described above constitutes a satisfactory basis for the creation of an effective industrial technology for the preparation of a large class of high-temperature non-metallic materials on which progress in many modern branches of engineering and industry depends significantly.

The method has also many possibilities for scientific research at high temperatures: in the study of chemical reactions in the melt, heterophase equilibria, the physical and physicochemical properties of melts, etc., and also for studies on the chemistry of high-temperature materials.

Not only the final products but also fused half-finished articles for use in the growing of sapphire, garnet, etc. single crystals and in glassmaking by traditional methods can be obtained by means of the technology involving fusion in a cold container.

REFERENCES

1. J. Czochralski, Z. phys. Chem., 92, 219 (1917).
2. W. V. Bolton, Z. Elektrochem., 11, 45 (1905).
3. A. A. Neustruev and G. L. Khodorovskii, "Vakuumnye Garnissazhnye Pechi" (Lined Vacuum Furnaces), Izd. Metallurgiya, Moscow, 1967.
4. A. A. Fogel', Izv. Akad. Nauk SSSR, Metallurgiya i Toplivo, No. 2, 24 (1959).
5. G. H. Schippereit, J. Metals, 13, No. 2, 140 (1961).
6. H. F. Sterling and R. W. Warren, Metallurgia. The Brit. J. of Metals, 67, No. 404, 301 (1963).
7. L. L. Kochergin, A. E. Slukhotskii, A. S. Vasil'ev, and Yu. B. Petrov, USSR P. 138755 (1960); Byul. Izobret., No. 11, 52 (1961).
8. F. K. Monforte, J. Appl. Phys., 32, 959 (1961).
9. G. W. Clark and A. T. Chapman, International Symposium, Dresden, 1965, p. 6.
10. French P. 1 358 438 (1963); "Bulletin officiel de la Propriete industrielle", No. 16, 1964.
11. French P. 1 430 962 (1964); "Bulletin officiel de la Propriete industrielle", No. 11, 1966.
12. Yu. B. Petrov and E. A. Bezrukova, Izv. Akad. Nauk SSSR, Ser. Neorg. Materialy, 4, 1162 (1968).
13. V. I. Aleksandrov, V. V. Osiko, A. M. Prokhorov, and V. M. Tatarintsev, "Current Topics in Materials Science" (Edited by E. Kaldis), North Holland Publ. Co., 1978, Vol. 1.
14. V. I. Aleksandrov, V. V. Osiko, and V. M. Tatarintsev, "Otchet FIAN" (Report of the Physical Institute of the USSR Academy of Sciences), Moscow, 1968.
15. V. I. Aleksandrov, V. V. Osiko, A. M. Prokhorov, and V. M. Tatarintsev, Vestnik Akad Nauk SSSR, No. 12, 29 (1973).
16. Yu. A. Polonskii, E. R. Skue, V. I. Mogilenski, V. M. Ganyuchenko, and Yu. B. Petrov, Ogneupory, No. 7, 26 (1973).
17. J. F. Wenckus, "Study, Design and Fabrication of a Cold Crucible System", Scientific Report, Boston, No. 1, 15 May 1974.
18. A. M. Vainberg, "Induktsionnye Plavil'nye Pechi" (Induction Fusion Furnaces), Gosenergoizdat, Moscow–Leningrad, 1960.
19. V. A. Donskaya (Editor), Handbook, "Vysokochastotnaya Elektrotermiya" (High-Frequency Electrothermal Processes), Izd. Mashinostroenie, Moscow–Leningrad, 1965.
20. J. A. Stratton, "Electromagnetic Theories" (Translated into Russian), Gostekhizdat, 1948.
21. B. R. Sundheim (Editor), "Fused Salts", McGraw Hill, New York, 1964.
22. G. V. Samsonov (Editor), Handbook, "Fiziko-Khimicheskie Svoistva Okislov" (Physicochemical Properties of Oxides), Izd. Metallurgiya, Moscow–Leningrad, 1965.
23. E. E. Shpil'rain, D. N. Kogan, L. S. Barkhatov, and L. I. Zhmakin, Teplofiz. Vys. Temp., 15, 423 (1977).
24. V. I. Aleksandrov, V. V. Osiko, and V. M. Tatarintsev, Izv. Akad. Nauk SSSR, Ser. Neorg. Materialy, 8, 956 (1972).
25. P. P. Budnikov and A. M. Ginstling, "Reaktsii v Smesyakh Tverdykh Vestchestv" (Reactions in Mixtures of Solid Substances), Stroiizdat, Moscow, 1971.
26. M. Foex, Rev. haute temp. refract., 3, 309 (1966).
27. W. M. Cohn and G. Braught, J. Opt. Soc. Amer., 44, 45 (1954).
28. M. Foex, "III Colloque national du Centre national de la recherche scientifique sur la chimie des hautes temperature", Paris, 1963, p. 177.
29. L. Ya. Ol'shanskii and V. P. Pryanishnikov, "Khimicheskaya Elektrothermiya" (Chemical Electrothermal Processes), Goskhimizdat, Moscow–Leningrad, 1962.
30. V. I. Aleksandrov, V. V. Osiko, V. M. Tatarintsev, and V. T. Udovenchik, Izv. Akad. Nauk SSSR, Ser. Neorg. Materialy, 9, 236 (1973).

31. V.N.Romanenko, "Poluchenie Odnorodnykh Poluprovodnikovykh Kristallov" (The Preparation of Homogeneous Semiconductor Crystals), Izd.Metallurgiya, Moscow, 1966.
32. V.I.Aleksandrov, V.V.Osiko, and V.M.Tatarintsev, Pribory i Tekh.Eksper., No.5, 222 (1970).
33. V.I.Aleksandrov, V.V.Osiko, and V.M.Tatarintsev, US P.3 824 302 (1971); US Department of Commerce Official Gazette of the United States Patent Office, 924, No.3, 651 (1974).
34. V.I.Aleksandrov, V.V.Osiko, and V.M.Tatarintsev, B.P.1 335 877 (1971); "Abridgments of Patent Specifications", H5, 1972.
35. V.I.Aleksandrov, V.V.Osiko, and V.M.Tatarintsev, French P.2122 768 (1971); "Bulletin officiel de la Propriete industrielle", No.35, 1972.
36. Z.N.Zonn and V.A.Ioffe, Symposium, "Rost Kristallov" (Crystal Growth), Izd.Nauka, Moscow–Leningrad, 1963, Vol.8, p.78.
37. V.A.Kuznetsov and O.V.Sidorenko, Kristallografiya, 13, 748 (1966).
38. V.I.Aleksandrov, V.V.Osiko, V.M.Tatarintsev, and V.T.Udovenchik, B.P.1 373 888 (1972); Chem. Abs., "Abridgments of Patent Specifications", C1, 1973.
39. V.I.Aleksandrov, G.E.Val'yano, B.V.Lukin, V.V.Osiko, A.E.Rautbort, V.M.Tatarintsev, and V.N.Filatova, Izv.Akad.Nauk SSSR, Ser.Neorg. Materialy, 12, 273 (1976).
40. V.I.Aleksandrov, E.E.Lomonova, A.A.Maier, V.V.Osiko, V.M.Tatarintsev, and V.T.Udovenchik, "Kratkie Soobshcheniya po Fizike (FIAN)" [Brief Communications on Physics (The Physical Institute of the USSR Academy of Sciences)], 1972, No.11, p.3.
41. F.A.Kroger, "The Chemistry of Imperfect Crystals" (Translated into Russian), Izd.Mir, Moscow, 1969.
42. V.I.Aleksandrov, V.F.Kalabukhova, E.E.Lomonova, V.V.Osiko, and V.M.Tatarintsev, Izv.Akad.Nauk SSSR, Ser.Neorg.Materialy, 13, 2192 (1977).
43. V.N.Vigdorovich, Yu.P.Adler, and V.V.Marychev, Izv.Vys.Ucheb.Zaved., Tsvetnaya Metallurgiya, No.3, 108 (1961).
44. V.I.Aleksandrov, Yu.K.Voron'ko, V.G.Mikhalevich, V.V.Osiko, A.M.Prokhorov, V.M.Tatarintsev, V.T.Udovenchik, and G.P.Shipulo, Dokl.Akad.Nauk SSSR, 199, 1282 (1971).
45. V.I.Aleksandrov, A.A.Kaminskii, G.V.Maksimova, A.M.Prokhorov, E.G.Sarkisov, A.A.Sobol', and V.M.Tatarintsev, Dokl.Akad.Nauk SSSR, 211, 567 (1973).
46. V.I.Aleksandrov, T.M.Murina, V.I.Zhekov, and V.M.Tatarintsev, "Kratkie Soobshcheniya po Fizike (FIAN)" [Brief Communications on Physics (The Physical Institute of the USSR Academy of Sciences)], 1973, No.2, p.17.
47. A.A.Kaminskii and V.V.Osiko, Izv.Akad.Nauk SSSR, Ser.Neorg.Materialy, 3, 417 (1967).
48. V.I.Aleksandrov, S.Kh.Batygov, Yu.K.Voron'ko, B.I.Denker, E.E.Lomonova, V.V.Osiko, and V.M.Tatarintsev, Izv.Akad.Nauk SSSR, Ser.Neorg. Materialy, 11, 664 (1975).
49. S.Kh.Batygov, Yu.K.Voron'ko, B.I.Denker, A.A.Maier, V.V.Osiko, V.S.Radyukhin, and M.I.Timoshechkin, Fiz.Tverd.Tela, 14, 977 (1972).
50. S.Kh.Batygov, R.G.Mikaelyan, V.V.Osiko, M.M.Fursikov, and V.T.Udovenchik, Izv.Akad. Nauk SSSR, Ser.Neorg.Materialy, 3, 760 (1967).
51. A.Anthony, Rev.Hautes Temp.Refract., 1966, No.2, p.147.
52. D.W.Strikler and W.G.Carlson, J.Amer.Ceram. Soc., 47, 122 (1966).
53. V.I.Aleksandrov, V.V.Voronov, Yu.S.Kuz'minov, V.V.Osiko, and V.M.Tatarintsev, "Kratkie Soobshcheniya po Fizike (FIAN)" [Brief Communications on Physics (The Physical Institute of the USSR Academy of Sciences)], 1975, No.3, p.3.
54. V.I.Aleksandrov, V.G.Gordon, V.L.Vinogradov, A.V.Dzhola, V.V.Osiko, E.G.Spiridonov, and V.M.Tatarintsev, "Kratkie Soobshcheniya po Fizike (FIAN)" [Brief Communications on Physics (The Physical Institute of the USSR Academy of Sciences)], 1976, No.6, p.10.
55. V.G.Gordon and E.G.Spiridonov, Ogneupory, No.5, 46 (1969).
56. V.I.Aleksandrov, V.F.Kitaeva, I.G.Kozlov, V.V.Osiko, N.N.Sobolev, V.M.Tatarintsev, and I.L.Chistyi, Kristallografiya, 18, 1085 (1973).
57. V.I.Aleksandrov, V.F.Kitaeva, I.V.Kozlov, V.V.Osiko, N.N.Sobolev, V.M.Tatarintsev, and I.L.Chistyi, Fiz.Tverd.Tela, 16, 2230 (1974).
58. V.I.Aleksandrov, V.F.Kitaeva, V.V.Osiko, N.N.Sobolev, V.M.Tatarintsev, and I.L.Chistyi, Fiz.Tverd.Tela, 1975, No.3, p.21.
59. I.L.Chisty, V.F.Kitaeva, and N.N.Sobolev, IEEE, J.Quant.Electr., 10, 888 (1974).
60. N.G.Pace, G.A.Saunders, Z.Samengen, and J.S.Thorp, J.Mater.Sci., 4, 1106 (1969).
61. V.F.Kitaeva and I.L.Chistyi, Pis'ma v Zhur. Eksper.Teor.Fiz., 13, 611 (1971).
62. D.F.Kiselev, T.M.Glushkov, and M.M.Firsova, Fiz.Tverd.Tela, 11, 3592 (1969).
63. I.I.Kitaigorodskii (Editor), "Tekhnologiya Stekla" (The Technology of Glass), Stroiizdat, Moscow, 1961.
64. B.Scott and H.Rawson, Glass Technol., 14, 115 (1973).
65. V.I.Aleksandrov, M.A.Borik, V.B.Glushkova, R.E.Krivosheev, N.I.Markov, V.V.Osiko, and V.M.Tatarintsev, Fiz.i Khim.Stekla, 3, 177 (1977).
66. O.K.Botvinkin and A.I.Zaporozhskii, "Kvartsevoe Steklo" (Quartz Glass), Stroiizdat, Moscow, 1965.
67. S.G.Tresvyatskii, USSR P.132 347 (1960); Byul. Izobret., No.19 (1962).
68. K.I.Portnoi and N.I.Timofeeva, Symposium, "Khimiya Vysokotemperaturnykh Materialov" (The Chemistry of High-Temperature Materials), Izd. Nauka, Leningrad, 1967, p.48.
69. M.Foex, Compt.rend., 260, 6389 (1965).
70. A.Anthony, G.Benezech, F.Cabannes, M.Faucher, M.Foex, Vutien Loc, and D.Yerouchalmi, "IIIrd International Symposium on High Temperature Technology, Asilomar, California, 1967", p.214.
71. R.Berjoan, A.Moise, M.Rivot, and J.P.Traverse, Science of Ceramics, 7, 343 (1973).
72. US.P 3 404 036 (1968); US Department of Commerce Official Gazette of the United States Patent Office, 855, No.1, 179 (1968).
73. B.P.1 142 798 (1968); "Abridgments of Patent Specifications", C1, 1969.
74. A.A.Lanin, Z.L.Koposova, E.D.Pivnik, G.G.Gavrik, V.I.Aleksandrov, V.V.Osiko, and V.M.Tatarintsev, USSR P.471 632 (1973); Byul.Izobret. No.19 (1975).
75. L.M.Ershova, B.V.Ignat'ev, L.P.Kusalova, E.E.Lomonova, V.I.Myzina, V.M.Tatarintsev, and L.G.Shcherbakova, Izv.Akad.Nauk SSSR, Ser.Neorg. Materialy, 13, 2042 (1977).

76. I.A.Surkova, N.M.Nikitina, V.L.Balkevich, D.N.Poluboyarinov, V.K.Garanin, V.V.Osiko, V.I.Aleksandrov, and V.M.Tatarintsev, Ogneupory, No.4, 40 (1977).
77. I.A.Surkova, R.Ruppelt, V.L.Balkevich, D.N.Poluboyarinov, V.K.Garanin, V.V.Osiko, V.I.Aleksandrov, and V.M.Tatarintsev, Izv.Akad. Nauk SSSR, Ser.Neorg.Materialy, 13, 712 (1977).
78. V.L.Balkevich, L.B.Borovkova, E.S.Lukin, D.N.Poluboyarinov, Z.O.Nemchenok, M.K.Titova, V.I.Aleksandrov, V.V.Osiko, and V.M.Tatarintsev, "Trudy MKhTI, Ser.Silikaty" (Transactions of the Moscow Institute of Chemical Engineering, The Silicate Series), Izd.Vysshaya Shkola, Moscow, 1973, No.72, p.61.
79. V.L.Balkevich, L.B.Borovkova, E.F.Lukin, D.N.Poluboyarinov, Z.O.Nemchenok, M.K.Titova, V.I.Aleksandrov, V.V.Osiko, and V.M.Tatarintsev, Ogneupory, No.4, 45 (1973).
80. F.A.K.Fekhredtinov, M.S.Molchanov, V.I.Aleksandrov, V.V.Osiko, and V.M.Tatarintsev, USSR P.482422 (1973); Byul.Izobret, No.32 (1975).
81. F.A.K.Fekhredtinov, M.S.Molchanov, V.I.Aleksandrov, V.V.Osiko, and V.M.Tatarintsev, Ogneupory, No.5, 57 (1976).
82. V.L.Balkevich, Yu.M.Mosin, V.V.Osiko, V.I.Aleksandrov, and V.M.Tatarintsev, Izv.Akad.Nauk SSSR, Ser.Neorg.Materialy, 11, 1335 (1975).
83. V.I.Aleksandrov, V.V.Voronov, V.F.Kalabukhova, Yu.S.Kuz'minov, and V.M.Tatarintsev, "Kraktie Soobshcheniya po Fizike (FIAN)" [Brief Communications on Physics (The Physical Institute of the USSR Academy of Sciences)], 1975, No.4, p.21.

The Physical Institute,
USSR Academy of Sciences,
Moscow